UNIVERSITY OF OKLAHOMA

GRADUATE COLLEGE

AFTERSHOCK DECAY IN SPACE AND TIME OF INDUCED SEISMICITY IN OKLAHOMA

A THESIS

SUBMITTED TO THE GRADUATE FACULTY

in partial fulfillment of the requirements for the

Degree of

MASTER OF SCIENCE

By

ZACHARY ROSSON
Norman, Oklahoma
2019

AFTERSHOCK DECAY IN SPACE AND TIME OF INDUCED SEISMICITY IN OKLAHOMA

A THESIS APPROVED FOR THE
CONOCOPHILLIPS SCHOOL OF GEOLOGY AND GEOPHYSICS

BY

Dr. Xiaowei Chen, Co-Chair

Dr. Jacob I. Walter, Co-Chair

Dr. Brett Carpenter

Acknowledgments

I was extremely lucky not only to have financial support for my degree, but to be surrounded by great people on all sides. Jake – thank you for being an excellent mentor the past two years. You helped me grow in science by never relenting in your high expectations of me. Pushing me to be independent and to think and communicate clearly has helped me grow tremendously, which I will undoubtedly carry into my professional life. Xiaowei and Thomas – thank you also for being great mentors and showing me how to do better science.

I am grateful for all the professors I learned from at OU and particularly the Geology & Geophysics department. Dr. C – thank you for being on my committee and being an excellent teacher. Thank you to the department staff, especially Rebecca, for making the logistics of my degree program go smoothly. Thank you to the geophysics graduate students and faculty group for facilitating great conversations at meetings and seminars and being easygoing and supportive.

I am appreciative of being able to be a research assistant at OGS and having opportunities with the seismic team as a result. Thank you to Joyce, Molly, Andrew, Peter, Fernando, Isaac, and Paul for being so easy to work with and bringing me into the team as a graduate student.

Most of all, I am thankful to have a loving and supportive family in Florida. To the Picking and Walser family in Tulsa, I am also grateful for all that you've done for me since I moved to Oklahoma. Lastly, to Courtney – you help me in more ways than you even realize. Thank you for being my partner and for supporting me steadfastly throughout my degree.

Table of Contents

List of Tables

List of Figures

Abstract

The current paradigm for estimating long-term seismic hazard in a region includes removing dependent earthquakes that occur after a mainshock, otherwise known as aftershocks, from an earthquake catalog to identify the underlying background Poissonian-like seismicity rate. In Oklahoma, attempts to quantify the seismic hazard are complicated by the 200-fold increase in the seismicity rate in the last decade, where 901 earthquakes of M3.0 and greater occurred in 2015 against a pre-2009 historical seismicity rate of just a few M3.0 and greater earthquakes per year. Thus, it is unclear how one would assess the current seismic hazard in Oklahoma with conventional methods for declustering. To examine the usefulness of declustered catalogs of Oklahoma seismicity in hazard modeling, one must first scrutinize the parameters used in the declustering procedures.

In this study, we work under the conceptual framework of identifying aftershocks using fixed space-time windows that are scaled by mainshock magnitude. We then use techniques to examine how aftershocks decay in space and time, and compile data-driven distance-time cutoffs which can be used as parameters for fixed-window declustering of Oklahoma seismicity. Our approach also allows us to observe that the decay of aftershocks in space is more rapid in Oklahoma than in Southern California, while the decay of aftershocks in time is indistinguishable between the two regions. These observations may suggest that Oklahoma has a smaller fractal dimension of its fault network and temporal aftershock decay controlled by induced pressure changes more than tectonic stresses. Most importantly, since inadequately parameterized aftershock identification windows can ultimately under- or over-estimate the regional seismic hazard, our results speak to the necessity of well-founded declustering parameters for seismic hazard assessment, especially in regions of induced seismicity.

Chapter 1: Introduction

A by-product of heightened unconventional oil and gas production in the central United States over the past decade has been the sharply rising and highly variable seismicity rates, mostly linked to the disposal of produced wastewater (Ellsworth, 2013). Most of the recent seismicity in the broader region has occurred in the state of Oklahoma, which has been characterized by high productivity swarms (Benz et al., 2015), elevated background rates (Walsh & Zoback, 2015), and four large mainshocks of *M* 5 and greater since 2011 (Chen et al., 2017; Goebel et al., 2017; McGarr & Barbour, 2017; McMahon et al., 2017; Walter et al., 2017; Yeck et al., 2017). Although the earthquake rate has been declining since 2016 in Oklahoma due to both market-driven reductions in new production wells in central Oklahoma and mandated regional wastewater injection rate reductions (Baker, 2017), it remains well above pre-2009 levels. Given these conditions, various researchers have attempted to forecast future seismic hazard for the state (Goebel et al., 2016; Langenbruch & Zoback, 2016; Langenbruch et al., 2018; Norbeck & Rubinstein, 2018; Petersen et al., 2016).

Past locations and rates of earthquakes are a key component of earthquake hazard forecasts. Probabilistic seismic hazard models in the United States have historically been developed using long-term seismicity rates and patterns of tectonically-driven background activity. Over long times, the occurrence of an event might be random within a given activity rate, such that the seismicity approaches a statistical Poissonian distribution (Cornell, 1968; Gardner & Knopoff, 1974; Petersen et al., 2016). The goal of such efforts are long-term or time-independent forecasts of future activity, requiring the removal of short-term rate bursts during aftershock sequences through different declustering techniques (van Stiphout et al., 2012). Recently published short-term U.S. Geological Survey (USGS) hazard forecasts for the central

U.S. use a space-time window declustering procedure from *Gardner & Knopoff* (1974), which was originally derived for Southern California (Petersen et al., 2016, 2017, 2018). In addition to mainshock-magnitude scaled space-time windows (Gardner & Knopoff, 1974; Uhrhammer, 1986), other commonly used declustering techniques include cluster-linking using assumptions about post-mainshock stress distributions (Reasenberg, 1985), stochastic declustering based on point processes (Zhuang et al., 2002), and non-parametric network-tree aftershock identification (Baiesi & Paczuski, 2004; Zaliapin et al., 2008).

In Oklahoma, both tectonic stresses and short-term variations in fluid-injection activity are thought to influence earthquake rates. As a consequence, some hazard models for Oklahoma incorporate physical changes of fluid pressure (Langenbruch et al., 2018) and fault stressing conditions (Norbeck & Rubinstein, 2018) in an effort to link seismicity with injection rate changes. These studies produce different results, partly because the forecasted seismicity rates are compared with different types of catalogs that are either not declustered (Langenbruch et al., 2018) or declustered using parameters in the *Reasenberg* (1985) method, which were derived from a California catalog (Norbeck & Rubinstein, 2018). A properly declustered catalog could allow for meaningful comparisons between otherwise differently constructed models or forecasts. Additionally, a declustered catalog might allow for clarity in understanding how external effects, such as pressure/stress changes drive background seismicity or lack thereof.

To date, declustering parameters have not been defined specifically for Oklahoma. We derive mainshock-magnitude dependent aftershock identification windows for recent seismicity in Oklahoma, using techniques from statistical seismology to study the aftershock decay directly. We focus on fixed windows since this is the common practice for declustering in probabilistic seismic hazard assessment. For comparison, we also study Southern California aftershocks since

this region has been used to derive multiple commonly applied declustering algorithms (e.g. Gardner & Knopoff, 1974; Reasenberg, 1985).

We first examine the spatial decay of stacked aftershocks near mainshocks and define new spatial windows for different magnitude ranges. We then fit Omori-Utsu *p*-values to the temporal decay of sets of individual sequences. We discuss complexities associated with defining aftershock duration in a region of variable seismicity rates and then use stacked aftershock catalogs in time to constrain time windows for different magnitude ranges. The spatial and temporal decay results lend themselves to interpretations of the physical and geologic setting of Oklahoma. Finally, we suggest declustering windows specific to Oklahoma seismicity and highlight the importance of constrained declustering parameters for understanding induced seismic hazard in Oklahoma and beyond.

Chapter 2: Data

For this study, we utilize earthquake catalogs from the Oklahoma Geological Survey (OGS) for 2009/01/01 to 2018/11/01 and from *Shearer et al.* (2005) via the Southern California Earthquake Data Center (SCEDC) for 1984/01/01 to 2003/01/01. This specific California catalog is used to validate our use of methodology from another study (Felzer & Brodsky, 2006) which used the same catalog.

The magnitude of completeness, M_c, is the lowest earthquake magnitude where 100% of the events in a given catalog are detected. A well-defined M_c is critical for statistical analysis of earthquake catalogs due to the heterogenous nature of data acquisition and processing within seismic networks (Gulia et al., 2012; Schorlemmer & Woessner, 2008). We estimate a single M_c

for each catalog by finding the point of maximum curvature of their frequency-magnitude distribution (Woessner & Wiemer, 2005) for 1000- and 5000- event-wide moving windows for Oklahoma and California, respectively. We take the median value over all windows to account for the time-varying M_c estimates, since overestimation reduces the amount of usable data and underestimation can lead to invalid results. We let M_c = 2.2 for Oklahoma and M_c = 1.5 for Southern California, which is applied uniformly in all analyses for both regions (Figure 1).

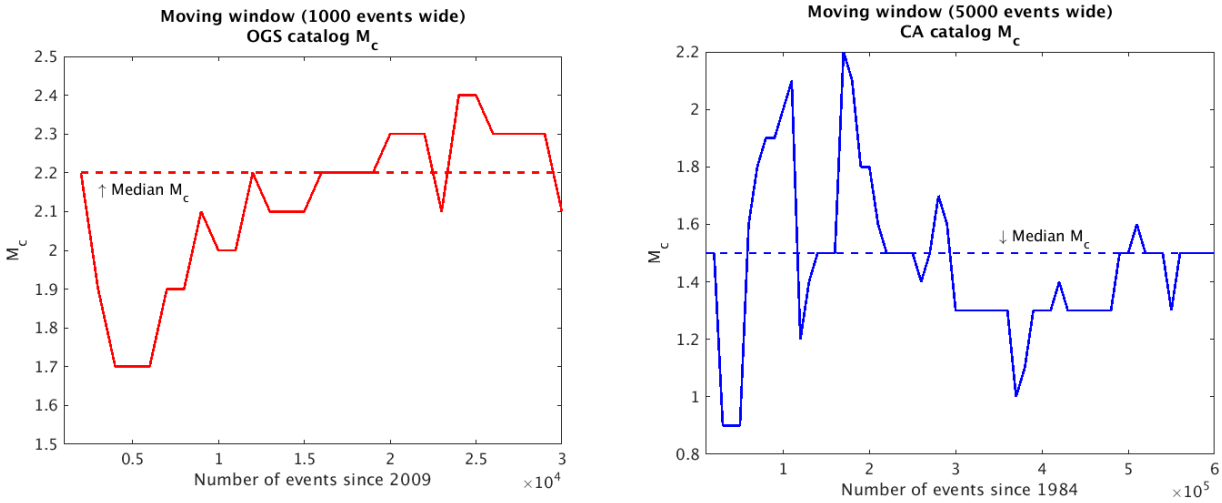

Figure 1. Magnitude of completeness (M_c) versus number of events in the OGS catalog and SCEDC catalog (Shearer et al., 2005).

Chapter 3: Spatial Aftershock Decay

In the following chapter, we describe the development of our stacked earthquake catalogs in space for Oklahoma and Southern California. We examine aftershock decay with distance during fixed time windows and compare the two regions. We then define spatial aftershock identification windows by separating aftershocks from background. Lastly, we interpret the physical and geologic meaning of our results.

3.1 Methods

Following *Felzer & Brodsky* (2006), we define clusters by segregating catalogs for mainshocks of a certain magnitude range and identifying neighboring earthquakes in time and space with fixed windows. We create composite catalogs of earthquakes associated with mainshocks by calculating epicentral distances from each windowed earthquake to its mainshock using the haversine great-circle formula. Cluster-specific sub-catalogs with distances recorded between earthquakes and the mainshock are stacked with all others in a mainshock magnitude range and sorted by distance to the common mainshock. Linear density, the number of aftershocks per unit length, is calculated between neighboring stacked earthquakes using the nearest-neighbor method (Silverman, 1986). The densities are calculated by taking the inverse of the differential distance between successive data points.

We also calculate median linear density values in log-spaced distance bins for each stacked catalog. Due to the high density of data points, the stacked spatial catalogs are visualized by creating a heat-map plot (Figure 2). We validate our overall stacking approach and density calculations by reproducing results from *Felzer & Brodsky* (2006) (Figure 3). We find agreement within the error bar of their study. Despite using the same techniques and dataset (Shearer et al.,

2005), slight differences in the decay rate likely emerge due to different curve fitting procedures and distance measurements (i.e. hypocentral versus epicentral distances).

In order to study the decay of primary aftershock sequences, we reduce contamination from other aftershock sequences by disqualifying potential mainshocks if larger earthquakes have occurred nearby in space and time. For Southern California, we require a distance separation of L = 100 km between mainshocks and for no larger earthquakes to occur within t_1 = 3 days before or t_2 = 0.5 days after potential mainshocks. For Oklahoma, we use the same time criteria, but require a distance separation of only L = 25 km between mainshocks given the paucity of earthquakes greater than M 6. The relative differences in spatial decay between the two regions are insensitive to increases in all three parameters (Table 1). Increasing t_1 has the greatest relative influence of the three parameters, yet the observed differences in decay rates for the two regions remains consistent.

We compile datasets of stacked earthquake linear density across space in Oklahoma and Southern California for multiple magnitude ranges and time windows. Earthquakes are selected within 250 km of each mainshock for time windows short enough to minimize background seismicity. Ideally, time windows of less than an hour should be chosen to reduce the effect of background seismicity and emphasize earthquakes possibly linked with a given mainshock. However, we use time windows from 1 to 72 hours for comparing the two regions, which represents a good trade-off between statistical robustness within the smaller dataset and the influence of background in Oklahoma (Table 2). The same time windows are used for both regions to minimize any biases due to window selection, since the number of stacked earthquakes and thus linear density values vary for different time windows in a given region.

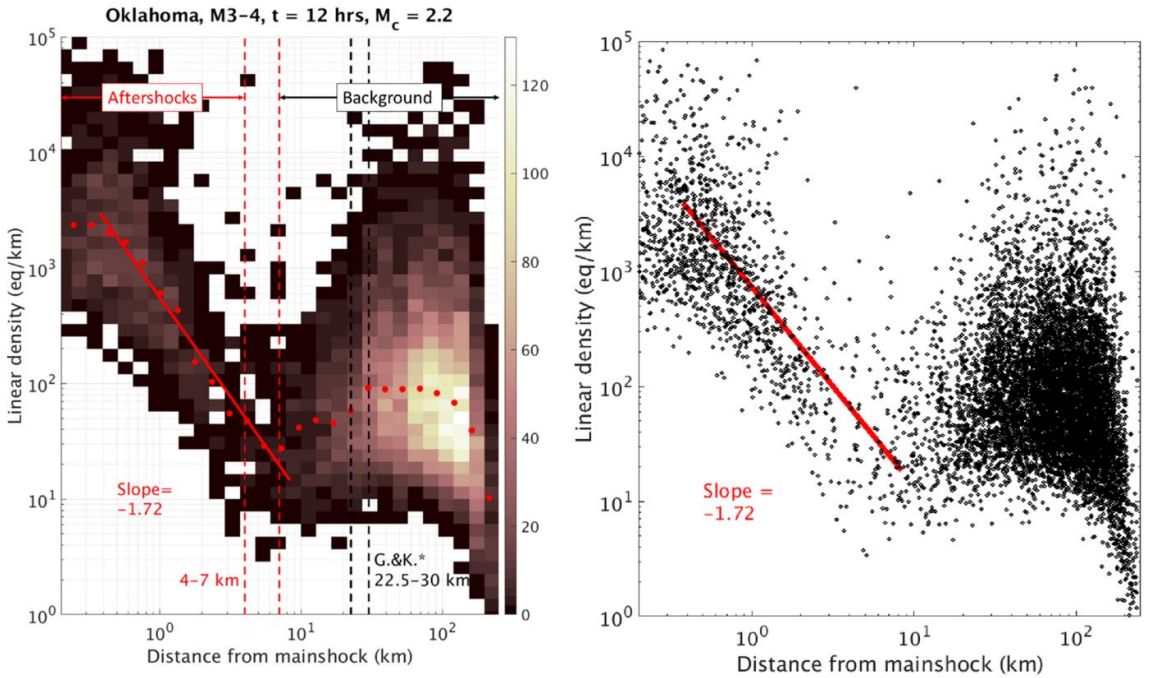

Figure 2. Example of spatial aftershock density data as visualized with a heat-map (left), populated by the original scatter plot density data (right).

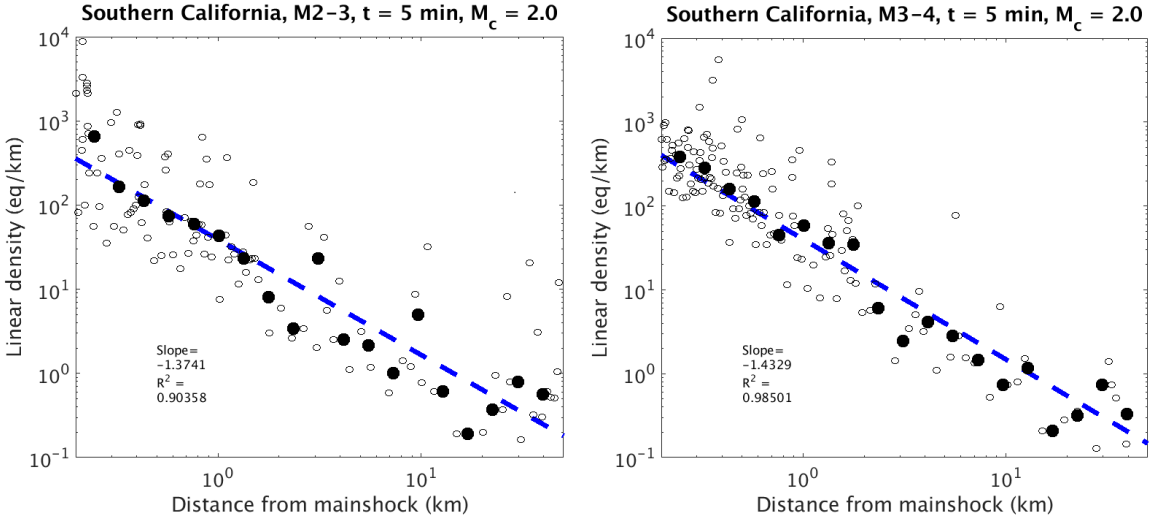

Figure 3. Linear density versus distance from stacked mainshocks, replicating the results of Figure 2 from *Felzer & Brodsky* (2006). Black dots are median linear density values in log-spaced bins. Black circles are stacked aftershocks. The decay is fit from 0.2 to 50 km using least-squares.

Oklahoma		
Parameters	Mainshocks *M* 3-4	Mainshocks *M* 4-5
L=25 km, t_1=3 days, t_2=0.5 days (Fig. 3-7)	-2.22 -> -1.72	-2.12 -> -1.96
L=25 km, t_1=3 days, t_2=0.5 days (Figs. 3-(3-5))	-1.72	-2.02
L=100 km, t_1=3 days, t_2=0.5 days	-1.78	-1.99
L=25 km, **t_1=30 days**, t_2=0.5 days	-1.92	-1.99
L=25 km, t_1=3 days, **t_2=3 days**	-1.72	-2.14
California		
Parameters	Mainshocks *M* 3-4	Mainshocks *M* 4-5
L=100 km, t_1=3 days, t_2=0.5 days (Fig. 3-7)	-1.44 -> -1.09	-1.20 -> -0.91
L=100 km, t_1=3 days, t_2=0.5 days (Figs. 3-(3-5))	-1.09	-0.91
L=250 km, t_1=3 days, t_2=0.5 days	-1.12	-0.96
L=100 km, **t_1=30 days**, t_2=0.5 days	-1.32	-1.51
L=100 km, t_1=3 days, **t_2=3 days**	-1.17	-0.98

Table 1. Spatial decay parameter tests for the same time windows as Figures 4-6 and Figure 8. Decay rates are compared for mainshocks of $3 \leq M < 5$ in both regions.

		Oklahoma		**California**	
Mainshock Magnitudes	Time (hours)	Mainshocks	Aftershocks	Mainshocks	Aftershocks
***M* 3-4**	1	1,663	1,051	2,351	2,712
	3	1,663	2,660	2,351	7,091
	6	1,663	4,916	2,351	13,404
	12	1,663	9,394	2,351	25,624
***M* 4-5**	6	61	440	255	4,317
	12	61	699	255	7,632
	18	61	954	255	10,781
	24	61	1,186	255	13,778
***M* 5-6**	72	4	266	38	12,951

Table 2. Number of mainshocks and aftershocks used in the spatial decay analysis for given mainshock magnitudes and time windows. The aftershocks column includes possible background events within 250 km of each mainshock.

3.2 Analysis and Results

For the stacked earthquake catalogs in Oklahoma and Southern California, the event density decay with distance from mainshocks allows for a qualitative separation of aftershocks and background. We fit an inverse power law using least-squares to the aftershock decay portion of the data. Mainshocks of $3 \leq M < 5$ in Oklahoma have more rapid aftershock decay with distance when compared to Southern California for the same time windows, where those power law exponents clearly differ by ~0.6-1.1 (Figures 4-6 and Figure 8).

We assess the statistical significance of this observation by conducting a two-sample Kolmogorov-Smirnov test. We find that stacked aftershock data from mainshocks of $3 \leq M < 5$ in the two regions are from different continuous distributions at the 1% significance level, indicating the difference in aftershock decay rates is statistically robust (Figure 7). Additionally, in Figure 7, we fit the aftershock decay in a least-squares sense to the raw data instead of the log-binned median values as in the rest of the spatial decay analysis. We find that fitting the raw stacked linear density data instead of the smoothed log-binned values has negligible effect, with decay rates differing by 0.09 at the most.

We also observe a relative difference in the distance range where aftershocks likely transition to background activity for the two regions. In general, mainshocks of $3 \leq M < 4$ for Oklahoma clusters are contained within a 4-7 km radius of the mainshock and Southern California clusters are contained within 15-20 km. For $4 \leq M < 5$, Oklahoma clusters are contained within 6-12 km and Southern California clusters are contained within 20-25 km. Since values of cluster window lengths are chosen only by visual inspection of event density changes with distance, we report a range of possible window lengths. This also allows us to factor

uncertainty into the measurements which in the following section are used to develop our spatial aftershock identification model.

To further evaluate the robustness of these results, we vary the time windows used to create the stacked aftershock datasets. These tests show that spatial aftershock decay is consistently more rapid in Oklahoma than in Southern California, although the decay rates decrease with increasing time due to gradual inclusion of background seismicity at all distances (Figure 8). Furthermore, Figures 26-29 of the Appendix contain the source plots of Figure 8, showing that although background rates may increase and flatten decay slopes, the inferred spatial aftershock windows are stable across time for given mainshock magnitude ranges.

Mainshocks of $5 \leq M < 6$ show the same overall behavior in Oklahoma with rapid spatial aftershock decay and tightly confined aftershock clustering (Figure 6). We have relatively fewer mainshocks in this magnitude range to analyze within Oklahoma (Table 2). Since M_c is important for evaluating the statistics of earthquake catalogs, we compute M_c for each of the four Oklahoma mainshocks individually. The rapid spatial aftershock decay of the larger events is qualitatively consistent with observations for the smaller mainshocks of $3 \leq M < 5$.

At short distances close to the stacked common mainshock, we observe flattening of density values (Figures 4 and 5), because larger earthquakes rupture across a spatial dimension within the same order of magnitude of the distances over which the aftershocks occur. Thus, we plot estimates for empirical subsurface rupture radii (Wells & Coppersmith, 1994) as a visual guide. As expected, we observe power law decay beyond those rupture radii for both regions as aftershocks influence regions beyond the coseismic rupture area.

Lastly, we test if higher location uncertainty in Oklahoma explains the observed differences in spatial decay using a high-resolution, waveform cross-correlated relocated Oklahoma catalog between 2013-2016 based on OGS catalog origin times (Schoenball & Ellsworth, 2017b). The median horizontal location uncertainty of the OGS catalog since 2009 is 0.90 km, while the same metric for the relocated catalog of *Schoenball & Ellsworth* (2017b) is only 0.22 km. If the observed differences between California and Oklahoma are indeed due to location uncertainty, we would expect the spatial decay to be more similar between California and Oklahoma for the relocated catalog. Our results are consistent with the decay observed in Figures 4 and 8, and thus suggest that the influence of relative location differences on spatial decay is insignificant in Oklahoma, because the location uncertainty is much smaller than the spatial decay window (Figures 9 and 10).

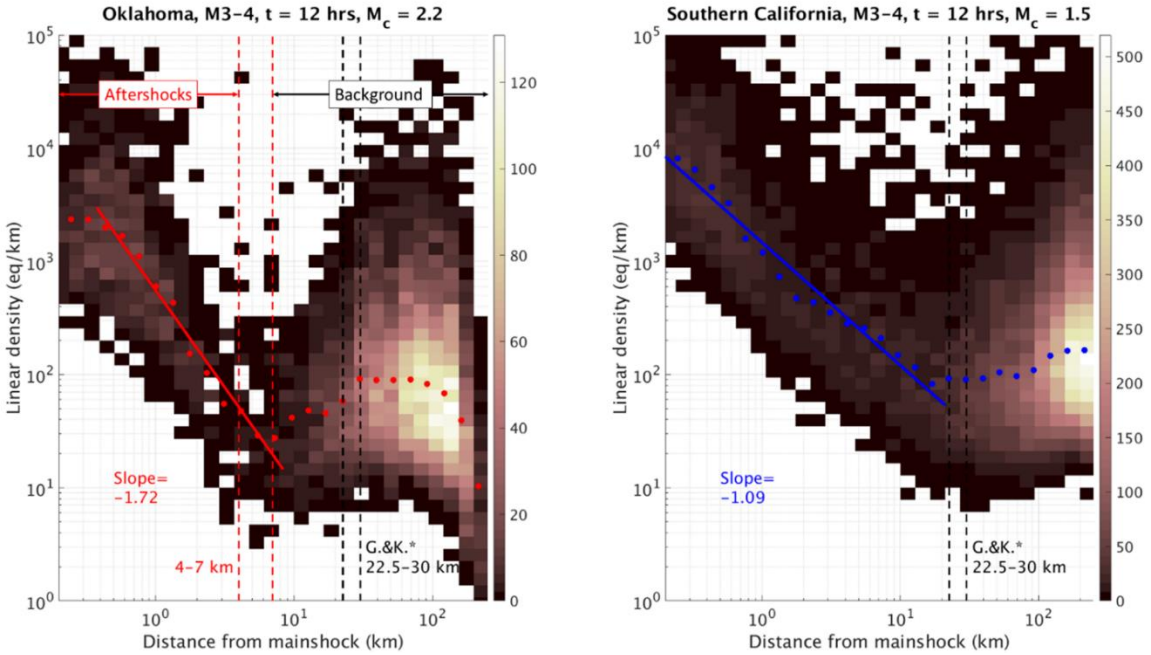

Figure 4. Linear event density versus distance from stacked mainshocks of $3 \leq M < 4$. Color bar shows the number of earthquakes in each grid. Aftershock decay is fit to the median linear density values in log-spaced bins (red and blue dots). Dashed black lines (G.&K.*) are spatial windows from *Gardner & Knopoff* (1974).

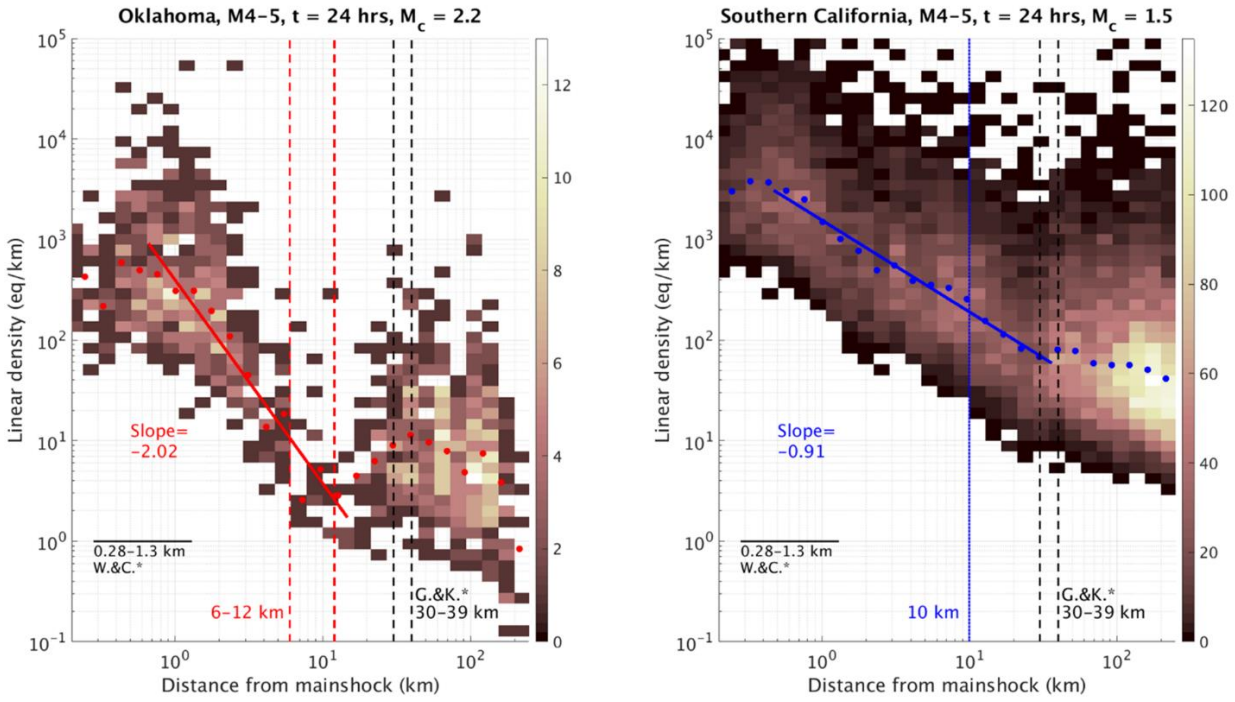

Figure 5. Linear event density versus distance from stacked mainshocks of $4 \leq M < 5$. Same plot components as Figure 4. Solid black lines (W.&C.*) are empirical subsurface rupture radii of mainshocks from *Wells & Coppersmith* (1994).

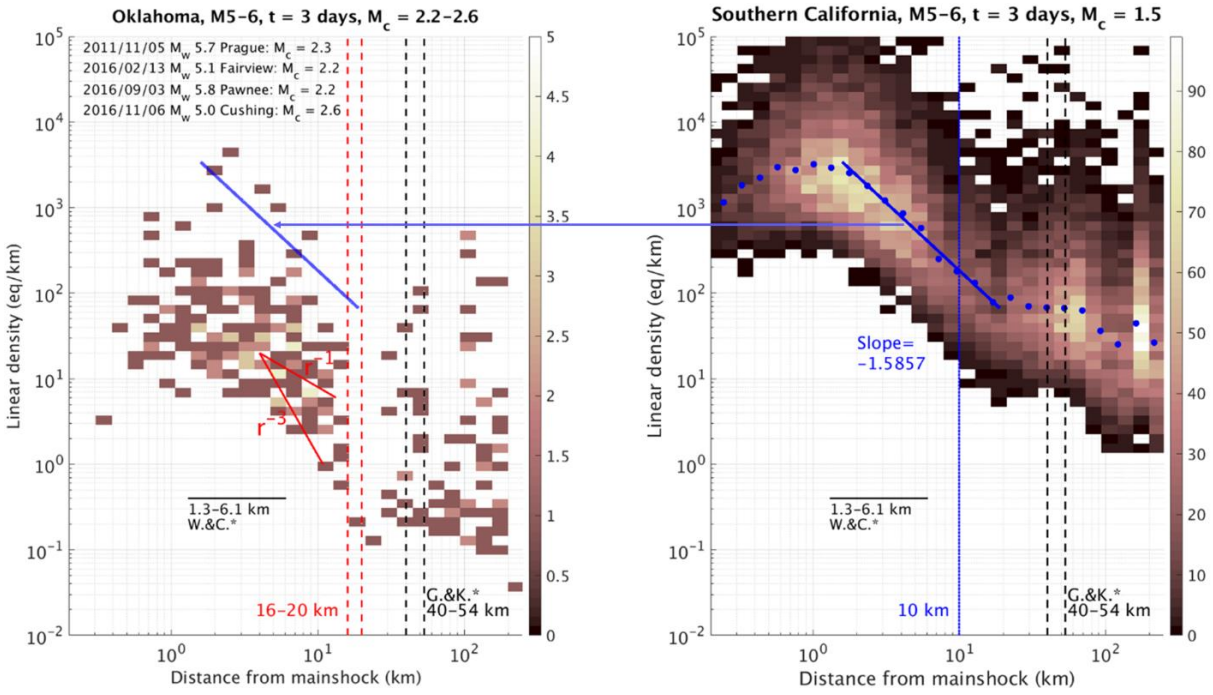

Figure 6. Linear event density versus distance from stacked mainshocks of $5 \leq M < 6$. Same plot components as Figure 5. The blue horizontal line transposes the Southern California aftershock decay to the Oklahoma panel for reference. We use separate M_c values for each of the four mainshocks in Oklahoma, determined by finding the point of maximum curvature of their frequency-magnitude distributions.

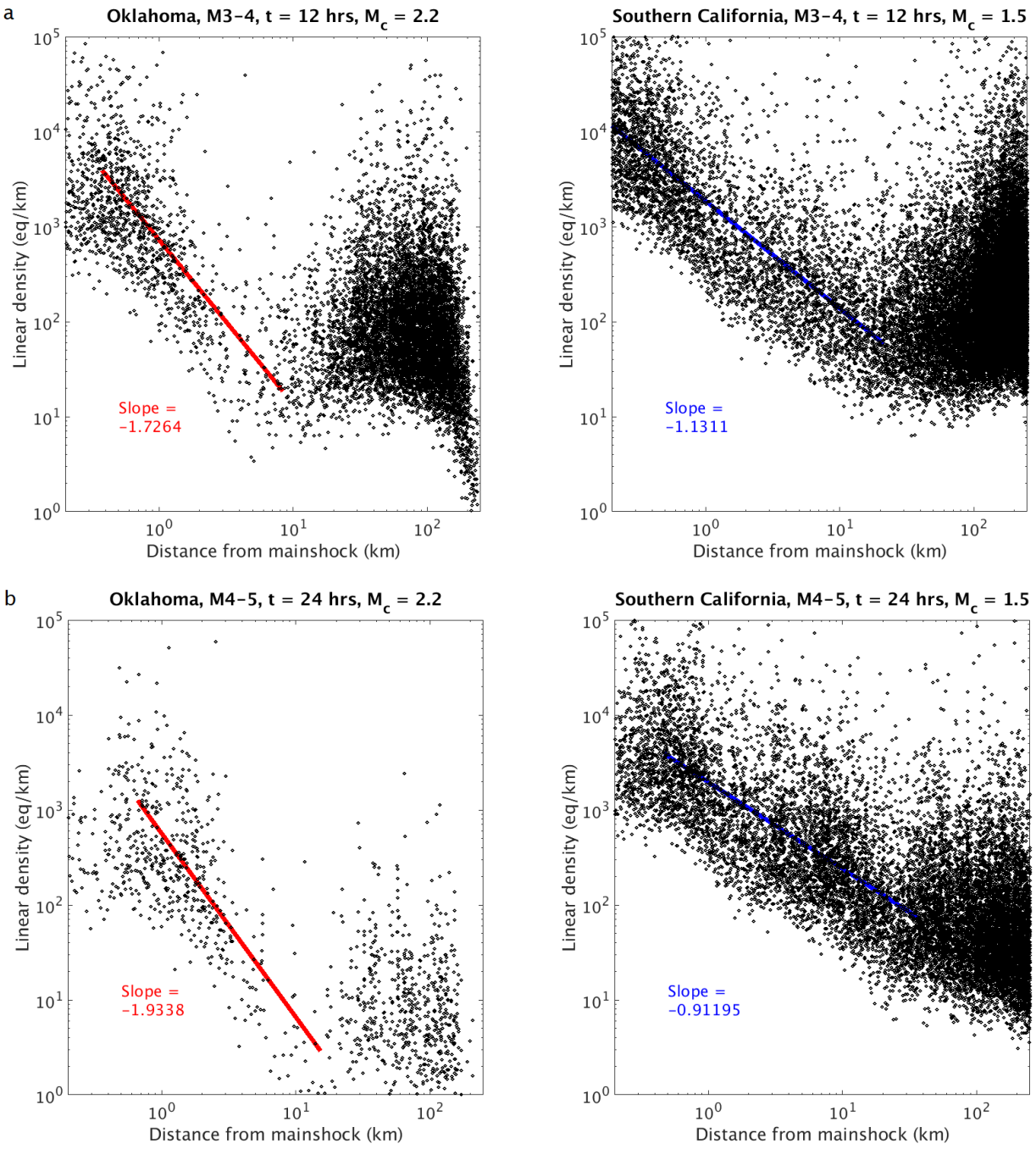

Figure 7. Linear event density versus distance from stacked mainshocks of a) $3 \leq M < 4$ and b) $4 \leq M < 5$. A two-sample Kolmogorov-Smirnov test between Oklahoma and Southern California for the two magnitude ranges shows that the difference in aftershock decay rates is statistically robust at the 1% significance level.

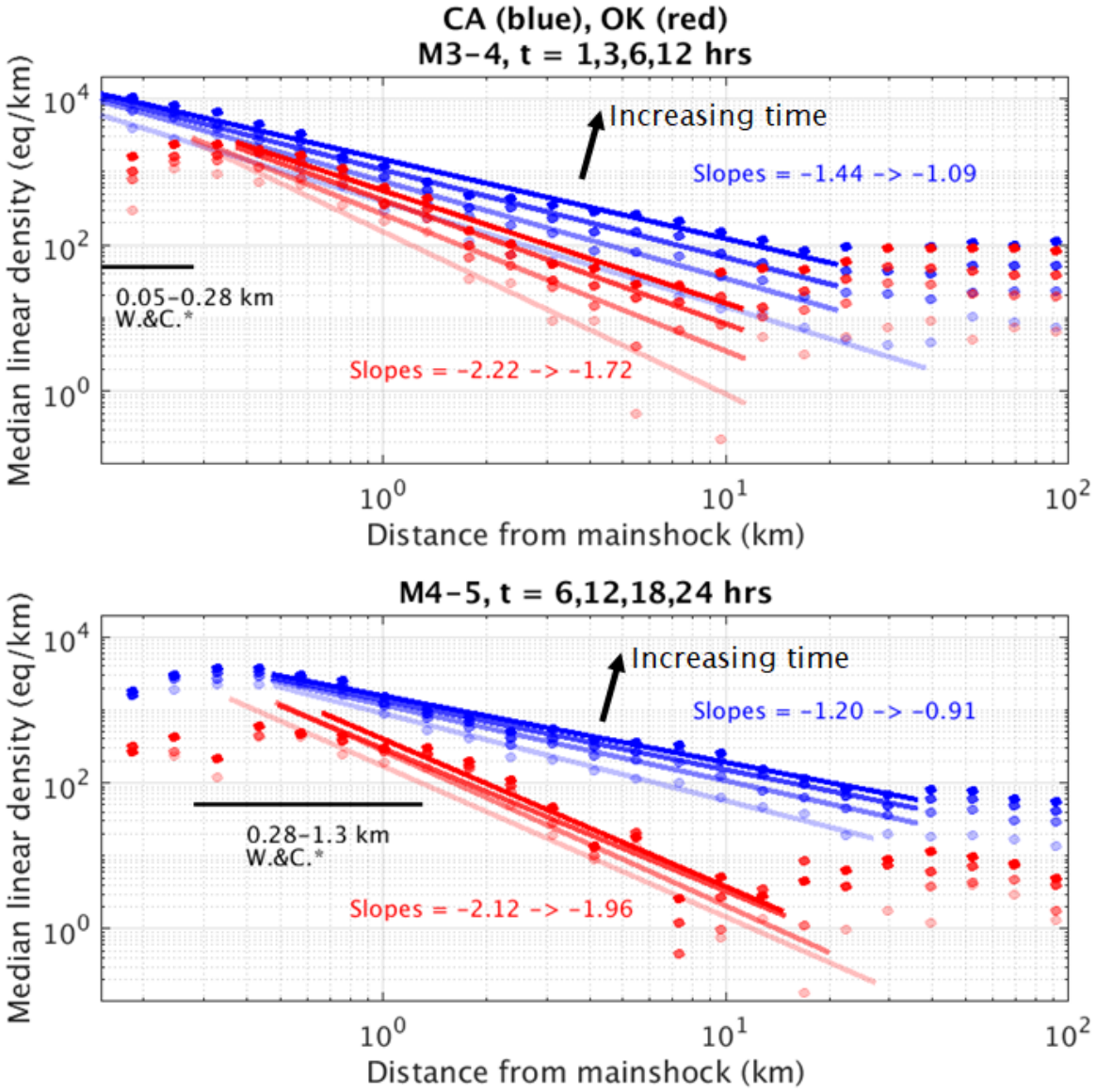

Figure 8. Median linear density of aftershocks versus distance from stacked mainshocks of $3 \leq M < 5$ for Oklahoma (red) and California (blue). Stacked aftershock catalogs are compiled for multiple short time windows (see Table 2), and lines which represent their decay increase in opacity with time as indicated by the black arrows. Solid black lines (W.&C.*) are empirical subsurface rupture radii of mainshocks from *Wells & Coppersmith* (1994).

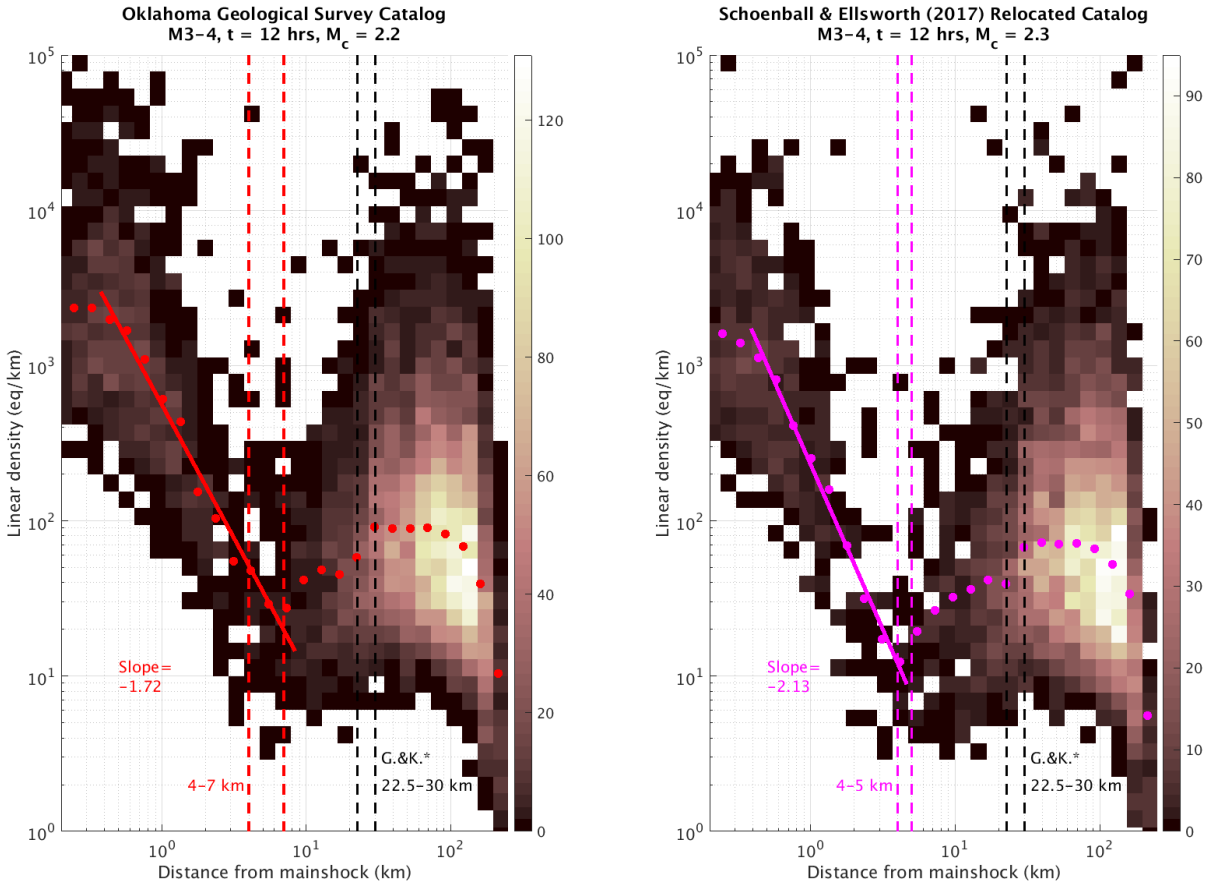

Figure 9. Linear event density versus distance from stacked mainshocks of $3 \leq M < 4$ for the catalogs from OGS and *Schoenball & Ellsworth* (2017b). Color bar shows the number of earthquakes in each grid. Aftershock decay is fit in a least-squares sense to the median linear density values in log-spaced bins (red and purple dots). Dashed black lines (G.&K.*) are spatial windows from *Gardner & Knopoff* (1974).

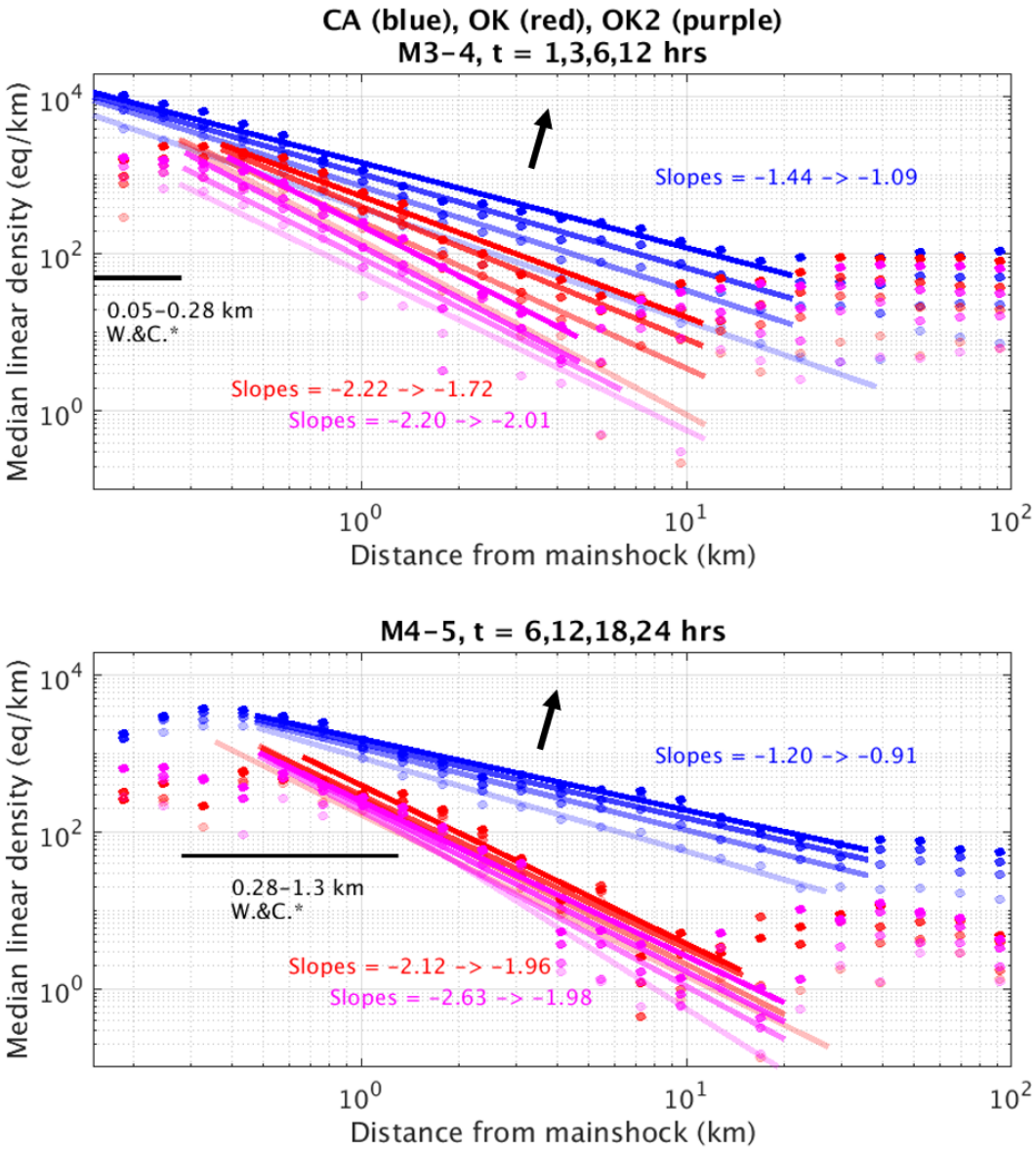

Figure 10. Median linear density of aftershocks versus distance from stacked mainshocks of $3 \leq M < 5$ for Oklahoma and California. Red: OGS catalog. Purple: *Schoenball & Ellsworth* (2017b) catalog. Blue: SCEDC (Shearer et al., 2005) catalog. Stacked aftershock catalogs are compiled for multiple short time windows, with the same plot components as in Figure 8.

3.3 Empirical Model for Spatial Windowing

Using our observations of inferred transition between aftershocks and background for a range of mainshock magnitudes, we determine a model for aftershock identification in space for Oklahoma (Figure 11). Given the range of distances expected to contain aftershocks for three magnitude bins in Figures 4-6 (red dashed lines), we plot spatial window radius versus mainshock magnitude. We populate the three boxes with a 0.1 km x 0.1 magnitude-unit mesh grid to obtain an unbiased distribution of possible aftershock windows. We then fit, in a least-squares sense, the distribution of the data (n=1463) as an increasing exponential function:

$$r = 10^{0.2217M-0.0227} \pm 2\delta \quad (1)$$

In Equation 1, *r* is the circular window radius in kilometers around a mainshock, *M* is the mainshock magnitude, and 2δ = 2.5585 km which is the 95% prediction interval of one tail of the distribution as derived from the standard error. The lower bound of this prediction interval allows for reasonable identification of aftershocks in Oklahoma with the lowest background contamination, which we apply in Chapter 4 to study temporal decay for long time periods:

$$r = 10^{0.2217M-0.0227} - 2.5585\ (km) \quad (2)$$

We also aim to reasonably constrain aftershock windows for Southern California to compare temporal aftershock decay with Oklahoma in Chapter 4. However, previous work has shown that the interconnected fault network in Southern California along the active plate boundary promotes productive secondary aftershock triggering (Marsan & Lengliné, 2010). These secondary aftershocks, in addition to background leakage, may significantly change the aftershock decay estimates (Marsan & Lengliné, 2010) and bias the inferred aftershock windows in the stacked density plots. As a result, a fixed window empirical model is not constructed for

California using the approach described above for Oklahoma. To reasonably identify aftershocks and reduce contamination for long time intervals in California, we let r = 10 km for $4 \leq M < 6$ as seen in Figures 5 and 6 (vertical blue lines).

3.3.1 Discussion

Issues of windowing and declustering in general are discussed further in Chapter 5. Here, we discuss specific possible limitations of our Oklahoma spatial windowing model. First, we use only *M* 3-6 mainshocks and their presumed aftershocks above a M_c of 2.2 to fit an equation of window radius versus magnitude. This requires extrapolation of expected windows for magnitudes below *M* 3 and above *M* 6. However, this approach may be sufficient since the USGS has only declustered mainshocks down to *M* 2.7 for Oklahoma (Petersen et al., 2016) and there is a paucity of *M* 6 and greater earthquakes in recorded Oklahoma history. Additionally, the 95% prediction interval (~ $\pm$ 2.6 km) in Equation 1 allows for uncertainties in aftershock identification for these smaller and larger mainshocks.

Second, we fit an increasing function scaled by mainshock magnitude like other windowing models (Gardner & Knopoff, 1974; Uhrhammer, 1986). This implies that the aftershock zone is driven by the mainshock rupture size. However, the physics of aftershocks and their distance decay is contested (e.g. Felzer & Brodsky, 2006; Richards-Dinger et al., 2010), which may affect interpretations of aftershock windows. In this study we analyze aftershock windows given many space-time parameters, but do not assume any physical triggering model and thus do not interpret the absolute values of the decay rates. The exponential behavior of Equation 1 is a by-product of the observed data. As a result, we assume that regardless of the physical mechanisms controlling the spatial aftershock decay, the mainshock magnitude is an adequate first-order control on aftershock window sizes for the purposes of declustering.

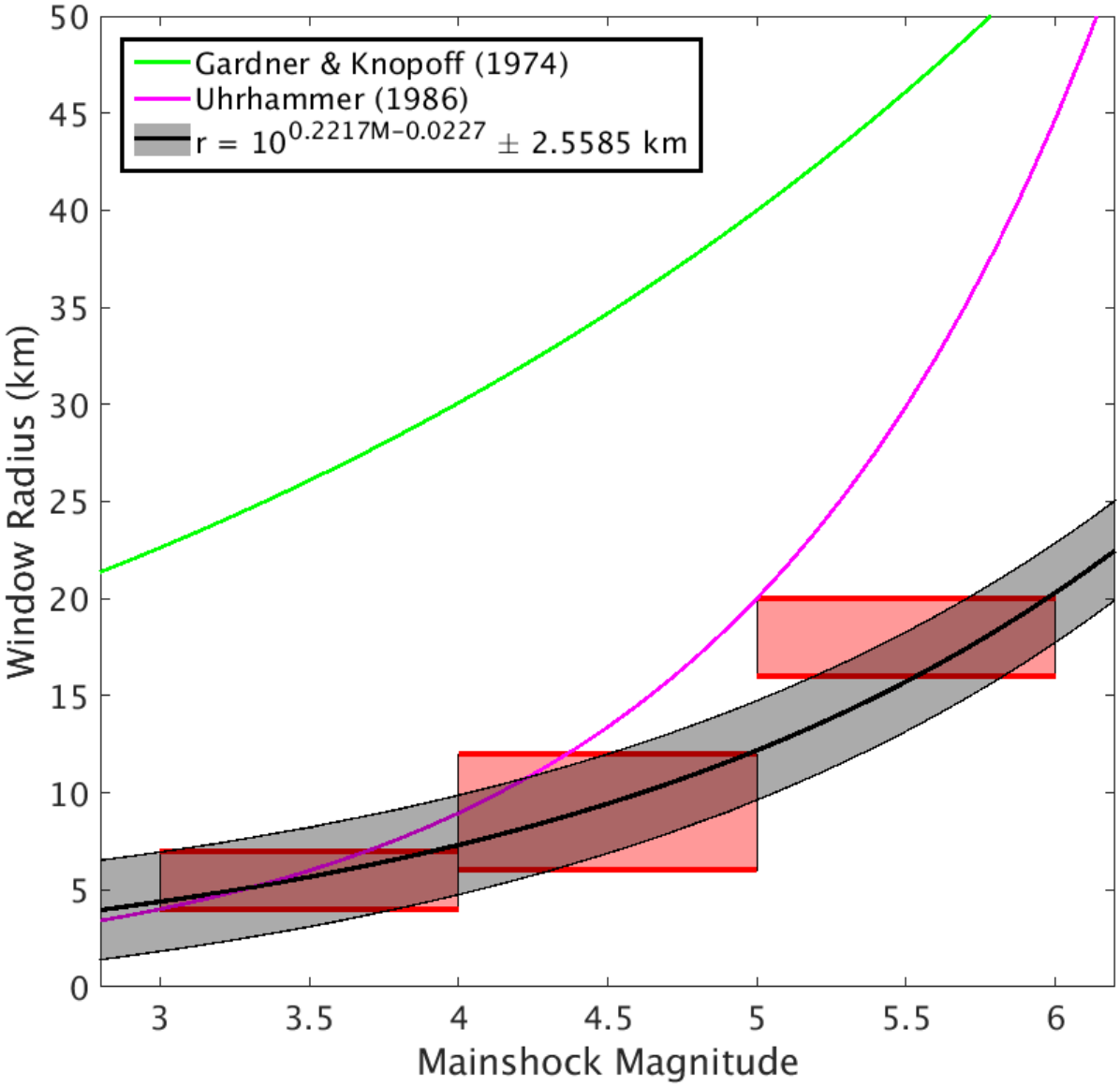

Figure 11. Spatial windowing model for Oklahoma aftershocks. Aftershock window ranges per mainshock magnitude are plotted as red boxes. The data points (n=1463), which are populated from three 0.1 km x 0.1 magnitude-unit mesh grids as described in Chapter 3.3, are fit to determine the parameters of Equation 1. Fixed windowing models of *Gardner & Knopoff* (1974) and *Uhrhammer* (1986) are compared.

3.4 Physical and Geologic Interpretations

We observe a significant and robust difference in spatial decay between Oklahoma and Southern California. Here we interpret physical significance of spatial aftershock decay and what our results may indicate about induced, intraplate seismicity in Oklahoma.

It is well accepted that most aftershocks occur on fault surfaces near the rupture zone of a mainshock (e.g. Helmstetter & Shaw, 2006; Kanamori & Brodsky, 2004), so that fault network properties can be inferred based on aftershock locations and statistics (e.g. Felzer & Brodsky, 2006; Schoenball & Ellsworth, 2017a). *Felzer & Brodsky* (2006) found that the spatial decay of aftershocks in Northern California was more rapid than in Southern California, possibly indicating a smaller fractal dimension of the fault network in Northern California. A similar explanation may be relevant when comparing Oklahoma to Southern California. However, work remains to estimate fractal dimensions of the active fault network in Oklahoma, possibly following the methods of *Pailoplee & Choowong* (2014) and *Wyss et al.* (2004).

Marsan & Lengliné (2010) found that the spatial decay of aftershocks in Southern California was highly sensitive to secondary aftershocks, and that removing them with a probabilistic linking method caused decay rates to increase significantly. These augmented Southern California decay rates of direct aftershocks are in line with our Oklahoma decay rates (-1.7 to -2.2). Although our methodologies and assumptions differ greatly, the results of *Marsan & Lengliné* (2010) speak to the inadequacy of windowing methods in regions with productive secondary aftershocks (see Chapter 5). However, the rapid spatial decay we observe in Oklahoma while still using a windowing method (which does not discriminate secondary aftershocks) may indicate that aftershock sequences in Oklahoma have reduced secondary triggering. It is plausible the observation is consistent with an intraplate setting with low tectonic

strain rates as observed by *Newman et al.* (1999), and disconnected fault patches as observed by *Shah & Crain* (2018) and *Schoenball & Ellsworth* (2017b). Southern California, on the other hand, has a mature fault network with interconnected splays of faults on an active plate boundary that promotes secondary triggering.

The interpretation of a smaller fractal dimension of the fault network and absence of abundant secondary aftershock triggering in Oklahoma is in line with recent studies which have shown that geologic structures act as significant controls on the evolution of induced seismicity (Pennington & Chen, 2017; Qin et al., 2018; Walter et al., 2017). These fault network interpretations may also support constraints on the possible maximum earthquake magnitude (M_{max}) for the region. *Chen et al.* (2018) found a truncated Gutenberg-Richter distribution of matched-filter data in Oklahoma, as seen from the absence of expected larger magnitude earthquakes in a given fault system, suggesting a lower M_{max}. Others have related the total injected wastewater volume in a given space-time interval to the maximum possible magnitude of induced earthquakes (Galis et al., 2017; McGarr, 2014). *Yeck et al.* (2015), however, suggested that the maximum magnitude was possibly controlled by both the cumulative injection volume and the geometry of the seismicity clusters.

Most likely, spatial aftershock decay depends simultaneously on the mainshock stress perturbation, the number of available adjacent faults close to failure, fault geometry and orientation, and aftershock triggering by static and dynamic stress changes. Thus, the observed rapid spatial decay in Oklahoma may be indicative of either fault network properties or the contribution of both induced and tectonic stresses. Distinguishing these two factors may be possible in the future with other well-recorded intraplate aftershock sequences in the central U.S.

Chapter 4: Temporal Aftershock Decay

In the following chapter, we describe how we compute temporal aftershock decay rates using *p*-values. We examine aftershock decay with time within fixed spatial windows and test the robustness of the results. We then discuss complexities associated with constraining aftershock durations in Oklahoma and introduce a novel method of estimating these durations. Lastly, we interpret the physical meaning of our results.

4.1 P-values

4.1.1 Methods

We analyze seismicity within 2 years after each mainshock of $4.5 \leq M < 6$ and use conservatively small spatial windows as described in Chapter 3.3 to define aftershock zones for both regions, using Equation 2 for Oklahoma and $r = 10$ km for Southern California. For each cluster, we systematically determine the Omori-Utsu parameters for aftershock decay with time (Omori, 1894; Utsu, 1969) following the modified Omori formula:

$$\frac{dn}{dt} = K(t + c)^{-p} \tag{3}$$

In Equation 3, *dn/dt* is the earthquake rate (in events/day), *t* is the time (in days) after the mainshock, *K* is the aftershock productivity, *c* is the completeness-time of aftershock detection, and *p* is the decay rate of aftershocks with time. To estimate the Omori parameters for each sequence, we use the maximum likelihood method following *Ogata* (1999) with a constrained optimization algorithm for nonlinear, multivariate functions. This procedure allows us to find optimized parameters for the statistical model using bounded constraints on *K* (5 - 300), *c* (0.02 - 2), and *p* (0.2 – 2.7).

4.1.2 Analysis and Results

Using conservatively chosen spatial windows (Chapter 3.3) and an identical procedure to estimate the Omori-Utsu parameters (Chapter 4.1.1), we use *p*-values as a relative metric of the temporal decay rate for sets of aftershock sequences. For mainshocks of $4.5 \leq M < 6$, we find median *p*-values of 0.78 and 0.83 for Oklahoma and California, respectively (Figure 12). We determine 95% confidence intervals for the two distributions of *p*-values using bootstrap resampling over 100 and 200 iterations for Oklahoma and California, respectively, and find that the distributions overlap (Figure 13). Overall, the temporal decay is statistically indistinguishable between the two regions.

To assess the robustness of our *p*-value results, we consider both data artifacts and properties of post-mainshock seismicity, which may bias our results. Each sub-catalog has 2 years of post-mainshock seismicity and significantly more data per sequence than in the spatial decay analysis. The rapid spikes that appear at longer post-mainshock times in Figure 12, especially in Southern California, are likely due to secondary aftershock sequences. We remove sequences that contain any earthquakes greater than or equal in magnitude to the mainshock; however, this does not necessarily remove all spikes since bursts of seismicity within a broader aftershock sequence may occur due to secondary aftershocks with lower magnitudes than the original mainshock. Applying this condition does not change the original *p*-value observation (Figure 14). We also require sequences to have a maximum time separation of 5 days between the mainshock and the first aftershock as well as a minimum of 10 total data points. These values are arbitrary but test the general dependence of the Omori parameter estimation on the amount of data in a given sequence. For these requirements, our *p*-value results remain stable (Figure 15).

To determine whether the incomplete detection of aftershocks at short times after mainshocks influences the power law fit, we compare our *p*-value results for different fixed *c*-values in the Omori fitting. For c = 0.01, 0.05, 0.1, 0.5, and 1 day, our median *p*-values are within the bootstrap resampling error of the median *p*-value determined for maximum likelihood estimated *c*-values, which vary per sequence (Figure 16). We also vary the time window for aftershock identification to 1 year and 6 months, respectively, which does not measurably impact the results (Figures 17 and 18). However, upon changing the spatial window from our refined model to that derived by *Gardner & Knopoff* (1974) we find that the original median *p*-values of 0.78 and 0.83 for Oklahoma and California decrease to 0.46 and 0.52, respectively (Figure 19). This flattening is due to the inclusion of unassociated background seismicity outside of the inferred aftershock zone. This finding highlights the sensitivity of temporal decay rates to the spatial windowing parameters used.

Through robustness testing (Figures 14-19) we find that our *p*-value estimates are largely insensitive to all parameters except the spatial window. We also observe through our *p*-value analyses some additional properties of the seismicity as follows. Both regions exhibit wide-ranging temporal decay with Southern California showing the greatest variation; visually, this is due to trade-offs between the productivity K, and time-completeness, c. Furthermore, Southern California shows prevalent secondary aftershock activity as evident from the seismicity spikes across time for many of the sequences. Secondary aftershocks may flatten the decay rates of some of the sequences, which illustrates the drawbacks of using spatial windows in such a region as described in Chapter 3.3. However, given the wide-ranging variability of decay as illustrated in Figure 13, removing such sequences may have a limited effect when comparing the distribution of *p*-values with that of Oklahoma which has few independent observations (n=11).

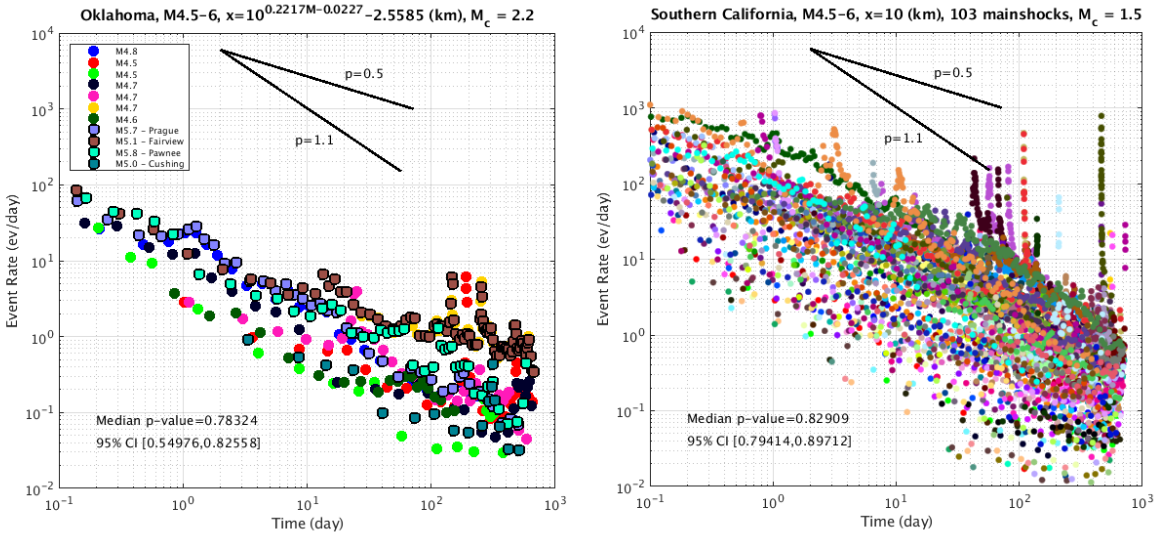

Figure 12. Temporal decay of sets of individual aftershock sequences with mainshocks of $4.5 \leq M < 6$. Black decay lines show references *p*-value slopes.

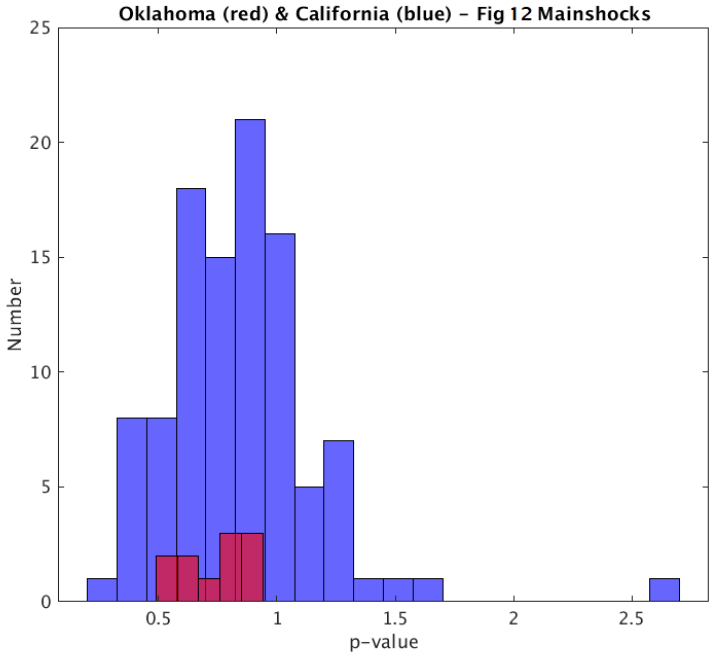

Figure 13. Histogram of *p*-values for mainshock-aftershock sequences in Figure 12.

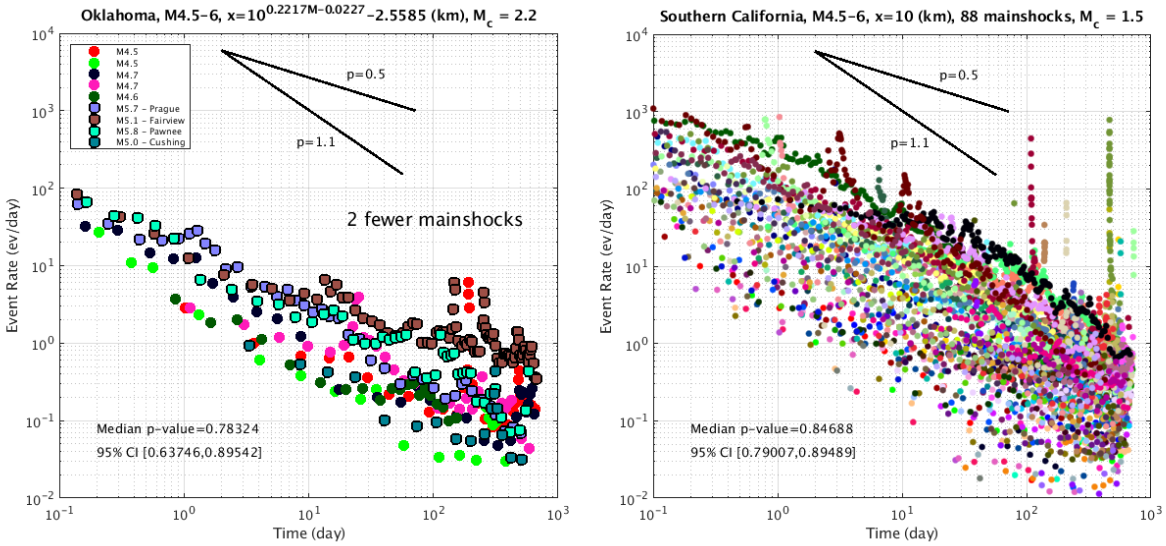

Figure 14. Same plot components as Figure 12. In this case, candidate mainshock-aftershocks with secondary activity that is equal to or larger in magnitude than the mainshock are removed.

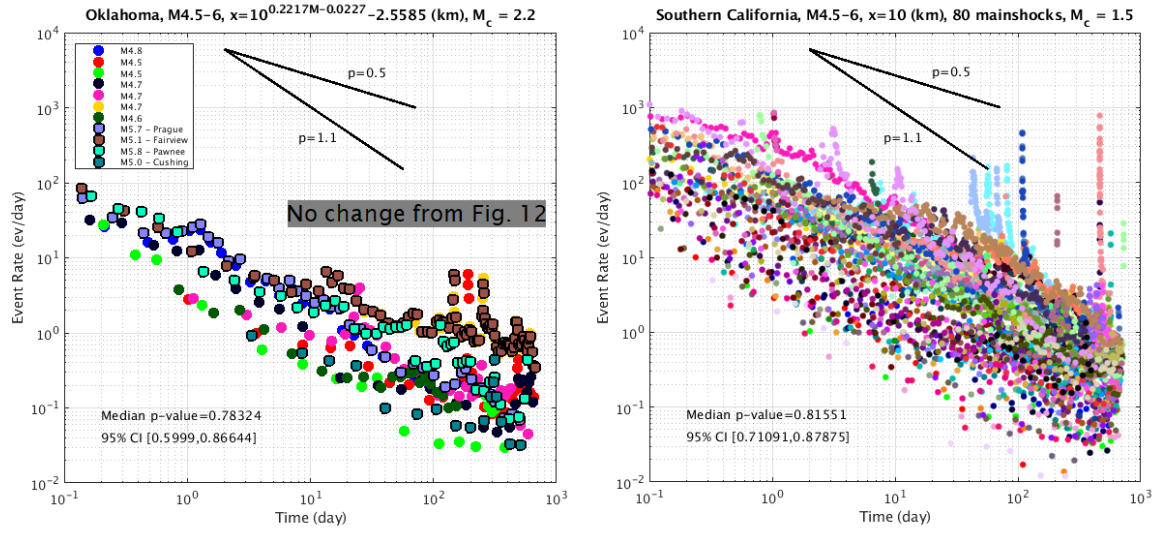

Figure 15. Same plot components as Figure 12. In this case, a maximum time separation of 5 days between the mainshock and first aftershock as well as a minimum of 10 total data points is required for any candidate mainshock-aftershock sequence.

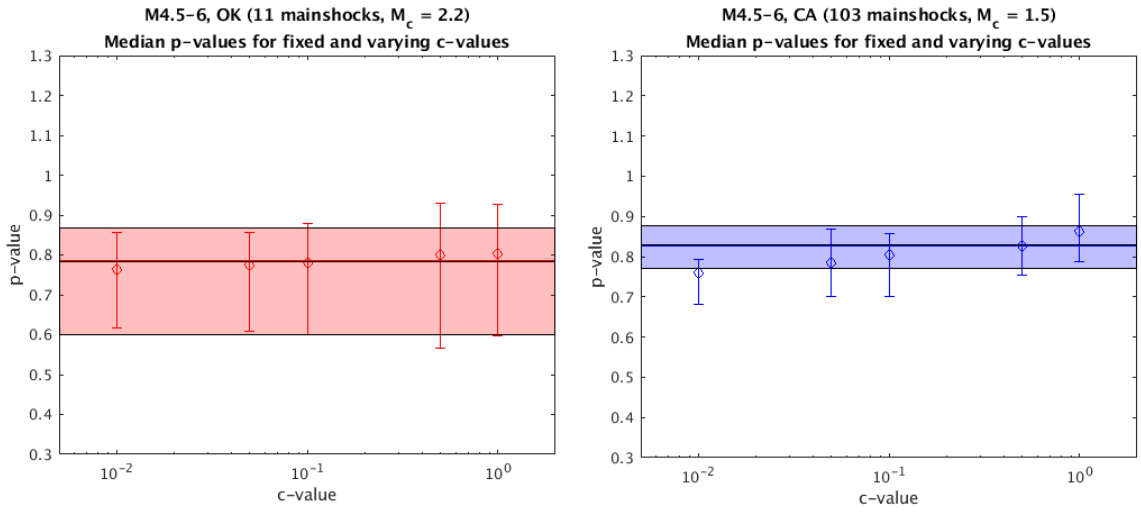

Figure 16. Five fixed *c*-values are used in the Omori fitting and compared with the default median *p*-value obtained with maximum-likelihood estimated *c*-values, which vary per sequence. 95% confidence intervals are determined for all *p*-value distributions around the median.

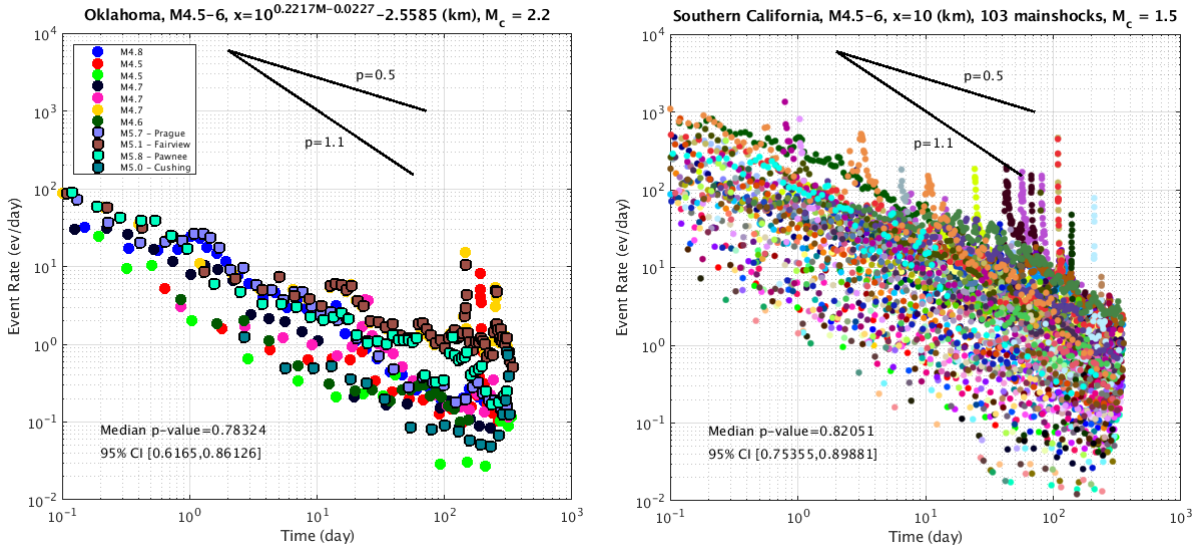

Figure 17. Same plot components as Figure 12. In this case, the time window is limited to 1 year after each mainshock.

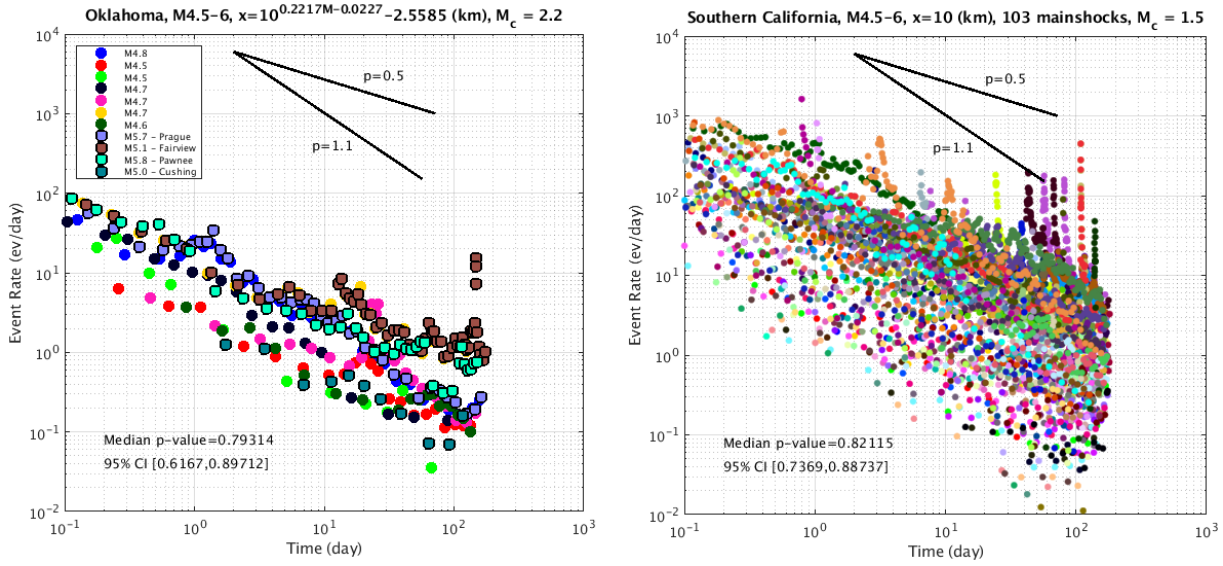

Figure 18. Same plot components as Figure 12. In this case, the time window is limited to 6 months after each mainshock.

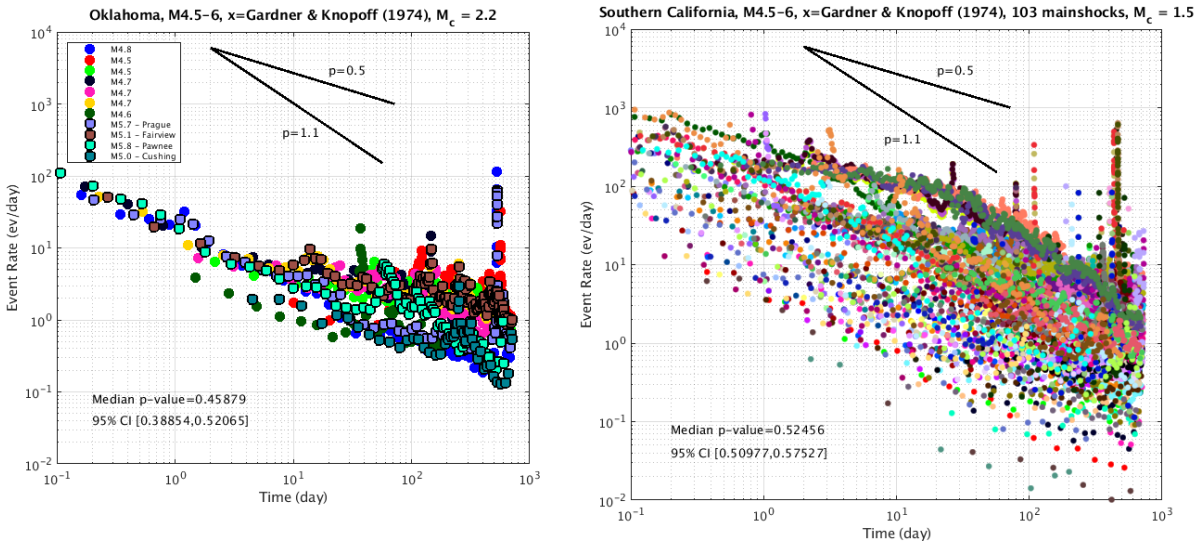

Figure 19. Same plot components as Figure 12. In this case, spatial windows from *Gardner & Knopoff* (1974) are applied for each mainshock for a time window of 2 years.

4.2 Temporal Aftershock Stacking

Establishing aftershock time windows is essential for declustering. However, the above *p*-value results do not produce robust conclusions about unique aftershock periods in Oklahoma. Wide-ranging and indistinguishable temporal decay observed between Oklahoma and Southern California does not convincingly establish that time windows used in Southern California should be used in Oklahoma. Here we introduce the difficulties associated with resolving aftershock duration. Then, we describe a novel method of stacking aftershocks in time to estimate aftershock durations of given mainshock magnitudes and analyze the results.

4.2.1 Motivation

The rate-and-state model of fault friction (Dieterich, 1994), which forecasts fault property changes after earthquakes, is used for aftershock studies where fault loading rates and aftershock durations are considered inversely related (Stein & Liu, 2009). Using this model, low tectonic loading rates correspond to aftershock sequences of hundreds of years and greater in intraplate settings. Since the mid-continental U.S. has been shown to have negligible tectonic plate motion (Newman et al., 1999), the rate-and-state model would suggest that aftershock sequences of large tectonic mainshocks in the region could last hundreds of years. Although this notion is disputed (e.g. Toda & Stein, 2018; Ziv, 2006), the observational limits of testing the hypothesis (i.e. seismicity catalogs only beginning around 1900) reflect the inherent ambiguity in distinguishing aftershocks from background at long time scales in an intraplate setting like Oklahoma.

In addition to the inherent complications brought about by long-term aftershock triggering that make temporal windows ambigious, properties of induced seismicity in Oklahoma create further issues. Ideally, the intersection of aftershock decay with a constant background can

be used to define the aftershock duration. However, Oklahoma seismicity rates of the past decade are highly variable and mostly correlated with wastewater injection rate changes (Ellsworth et al., 2015; Llenos & Michael, 2013). Thus, establishing a constant background rate to compare with the aftershock decay is ill-defined. Additionally, aftershock rates in Oklahoma are not driven exclusively by tectonic fault loading rates as is assumed in the *Dieterich* (1994) model. Decreased injection rates due to market forces and mitigation measures, as well as other induced stress changes, may impact aftershock productivity across time. Due to all these factors, in the following two sections we use a data-driven approach with no assumptions of a regional background rate to define time windows for declustering of Oklahoma aftershocks.

4.2.2 Methods

To create stacked aftershock density catalogs in time for Oklahoma, we follow a similar approach to Chapter 3.1. Sub-catalogs of mainshocks of $4 \leq M < 6$ are defined using a time window of 2 years and spatial windows as listed in Table 3. The spatial window parameters include minimum distances to account for near-mainshock location errors and mainshock rupture lengths in Oklahoma (see Figures 5 and 6). For each sub-catalog, the relative times between each mainshock and its windowed aftershocks are calculated, and each sub-catalog within a specific mainshock magnitude bin is stacked with the common mainshock at $t = 0$ years. The stacked catalog is then sorted by time relative to the common mainshock, and earthquake linear density in time is calculated with the nearest-neighbor method (Silverman, 1986). The stacked temporal density data is visualized identically to the spatial data as a heat-map, with median linear density values in log-spaced bins outlining the overall decay over time.

In summary, the stacked data described above simply represents the linear density of earthquakes in time rather than space. However, there are two key methodological differences

since more earthquakes accumulate in t = 2 years of stacked data (Table 3) than in the spatial decay analysis where t = 1 to 72 hours. First, similar to Chapter 3.1, the linear density of earthquakes in time is calculated by taking the inverse of the differential distance between successive data points for mainshocks of $4.5 \leq M < 6$. However, we take a 5-data-point-wide moving-window across time to calculate density values for mainshocks of $4 \leq M < 4.5$ since this range has an order of magnitude more stacked events. This effectively smooths the data towards the highest densities.

Second, we apply the same parameters as in Chapter 3.1 to disqualify potential mainshocks if larger earthquakes have occurred nearby in space and time (L = 25 km, t_1 = 3 days, t_2 = 0.5 days). We use these values for consistency to compile the same mainshock dataset as in the stacked spatial decay analysis. In Chapter 3.1, we found that the spatial decay results were insensitive to small changes in these parameters (Table 1). However, we did not test time windows on the order of years since removing all sequences with seismicity spikes greater than M_c (either from foreshocks of other events or secondary aftershocks) greatly reduces the amount of usable stacked data. Also, removing these sequences in such a way assumes that the remaining mainshocks have only direct aftershocks for 2 years after each mainshock, which places an implicit constraint on aftershock durations. However, since we found reduced secondary triggering in Oklahoma, we find it reasonable to only remove sequences that contain earthquakes greater than or equal in magnitude to the mainshock within 2 years like in Figure 14. This removes large foreshocks or secondary activity that occur at times greater than the default values of t_1 and t_2 while reducing the number of assumptions about earthquake triggering chains in Oklahoma.

4.2.3 Analysis and results

To validate our approach, we first inspect if the observed stacked decay rates are consistent with our results using *p*-values (Chapter 4.1). For conservatively small spatial windows within the lower bounds of our preferred spatial aftershock model (Figure 11 and Table 3), we obtain decay rates of -0.69 and -0.59 for mainshocks of $4.5 \leq M < 5$ and $5 \leq M < 6$, respectively (Figure 20(b-c)). These values are below the median *p*-value obtained in Figure 12 of 0.78, but within the 95% confidence interval of 0.55 to 0.83. This flattening is likely due to a combination of background seismicity accumulating over long time periods, productive secondary aftershocks below the mainshock magnitude (Felzer et al., 2003), and stacking effects which multiply the aggregate times sampled in each figure (Felzer & Brodsky, 2006). Furthermore, others have observed that *p*-values of stacked sequences tend to be smaller than those derived for individual mainshock-aftershock sets (e.g. Schoenball & Ellsworth, 2017a; Utsu et al., 1995).

To examine the effect of spatial window size on the stacked temporal decay, we increase spatial window sizes for all three magnitude ranges (Figure 21). The decay rates are similar to Figure 20 and fall within 0.3-0.6, but only for shorter time intervals less than 2 years. At longer times, the observed decay flattens, similar to that observed in Figure 19 which contains *p*-values for large spatial windows in Oklahoma. The transition from dominant aftershock decay to equal background/aftershock rates is illustrated in Figure 22. In other words, this “kink” in the inverse power law decay behavior may represent the point in the aftershock period where the aftershock cluster and surrounding few kilometers of background events start to occur at a nearly constant rate. The intersection of these two modes could provide a reasonable estimation for the average aftershock duration for that mainshock magnitude range. The kink in the aftershock decay for

mainshocks of $4 \leq M < 5$ reasonably aligns with the *Gardner & Knopoff* (1974) time windows, originally derived for Southern California.

	Oklahoma		
Mainshock Magnitudes	Spatial Window (km)	Mainshocks	Aftershocks
***M* 4-4.5**	**0.7 - 4**	**41**	**2,055**
	0.7 - 7	39	2,945
	0.7 - 10	**38**	**3,845**
***M* 4.5-5**	**0.7 - 4**	**5**	**229**
	0.7 - 7	5	289
	0.7 - 10	**5**	**394**
***M* 5-6**	**2.5 - 12**	**4**	**901**
	2.5 - 17	4	971
	2.5 - 22	**4**	**1,222**

Table 3. Parameters and stacked catalogs used in Figures 20 and 21. Aftershocks column includes possible background events within 2 years after each mainshock. Green shaded rows correspond with data in Figure 20, while blue shaded rows correspond with data in Figure 21.

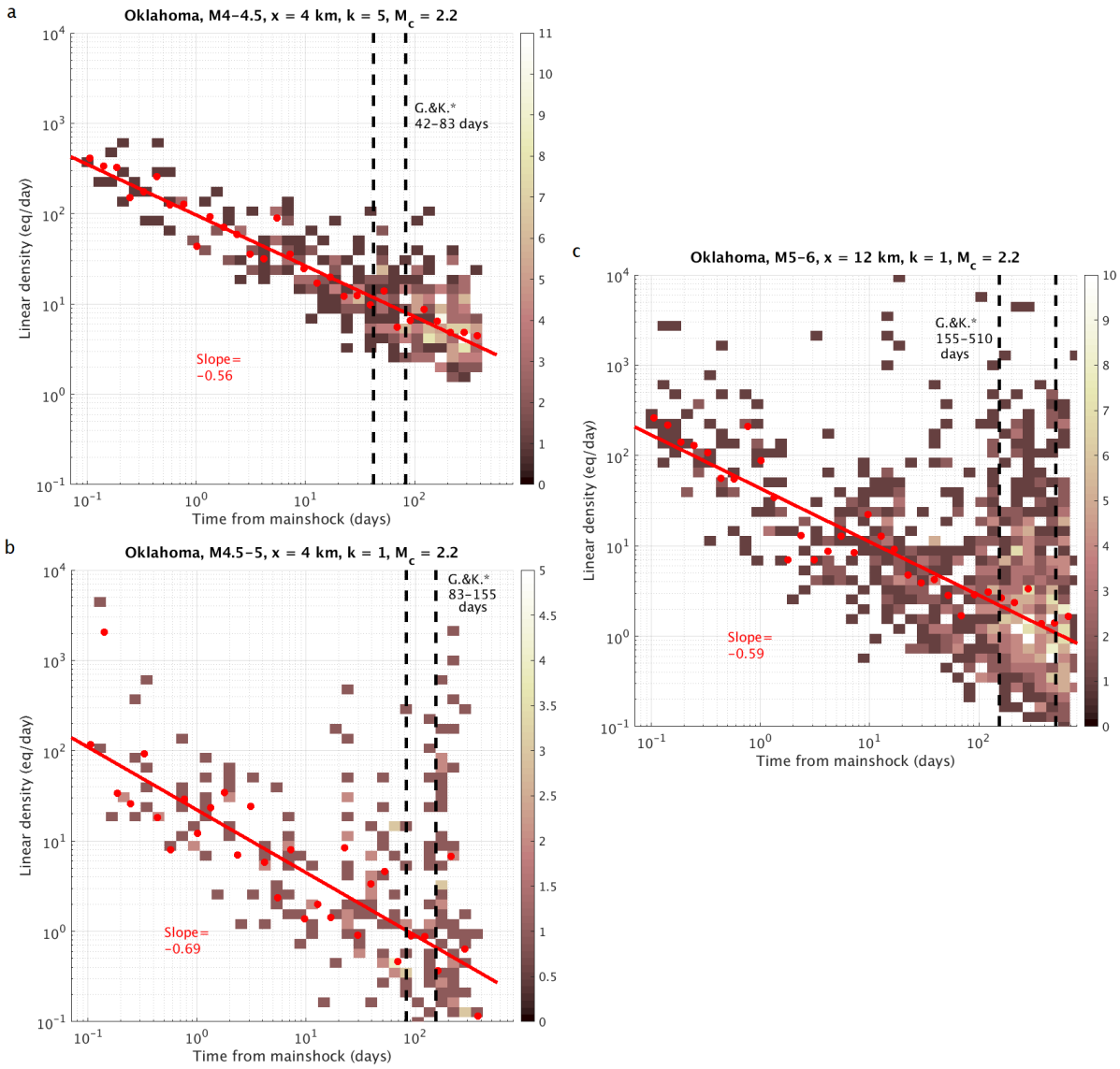

Figure 20. Aftershock linear density versus time from stacked mainshocks of (a) $4 \leq M < 4.5$, (b) $4.5 \leq M < 5$, and (c) $5 \leq M < 6$ in Oklahoma. Black dashed lines (G.&K.*) show time windows from *Gardner & Knopoff* (1974).

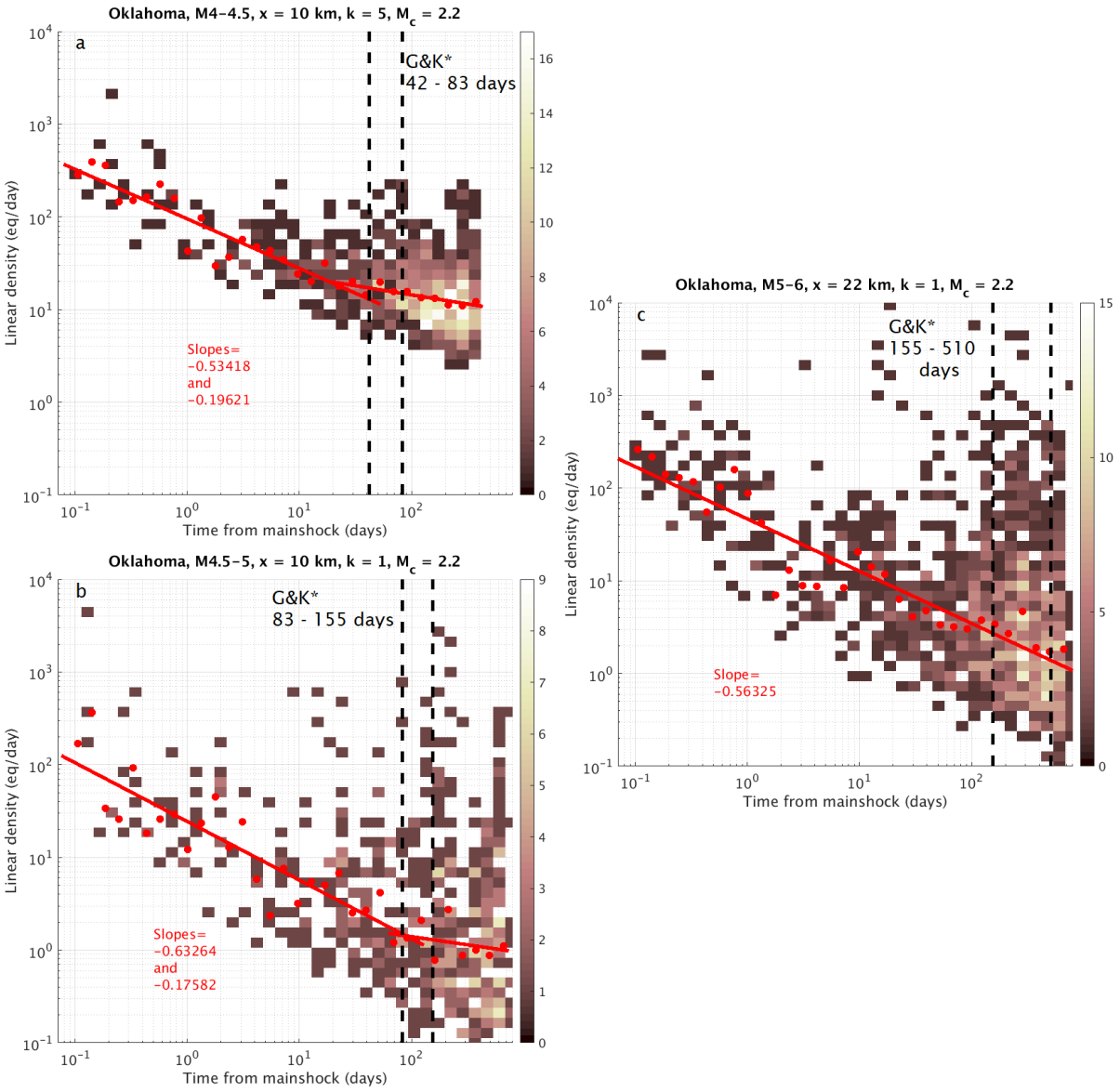

Figure 21. Same plot components as Figure 20, except for larger spatial windows.

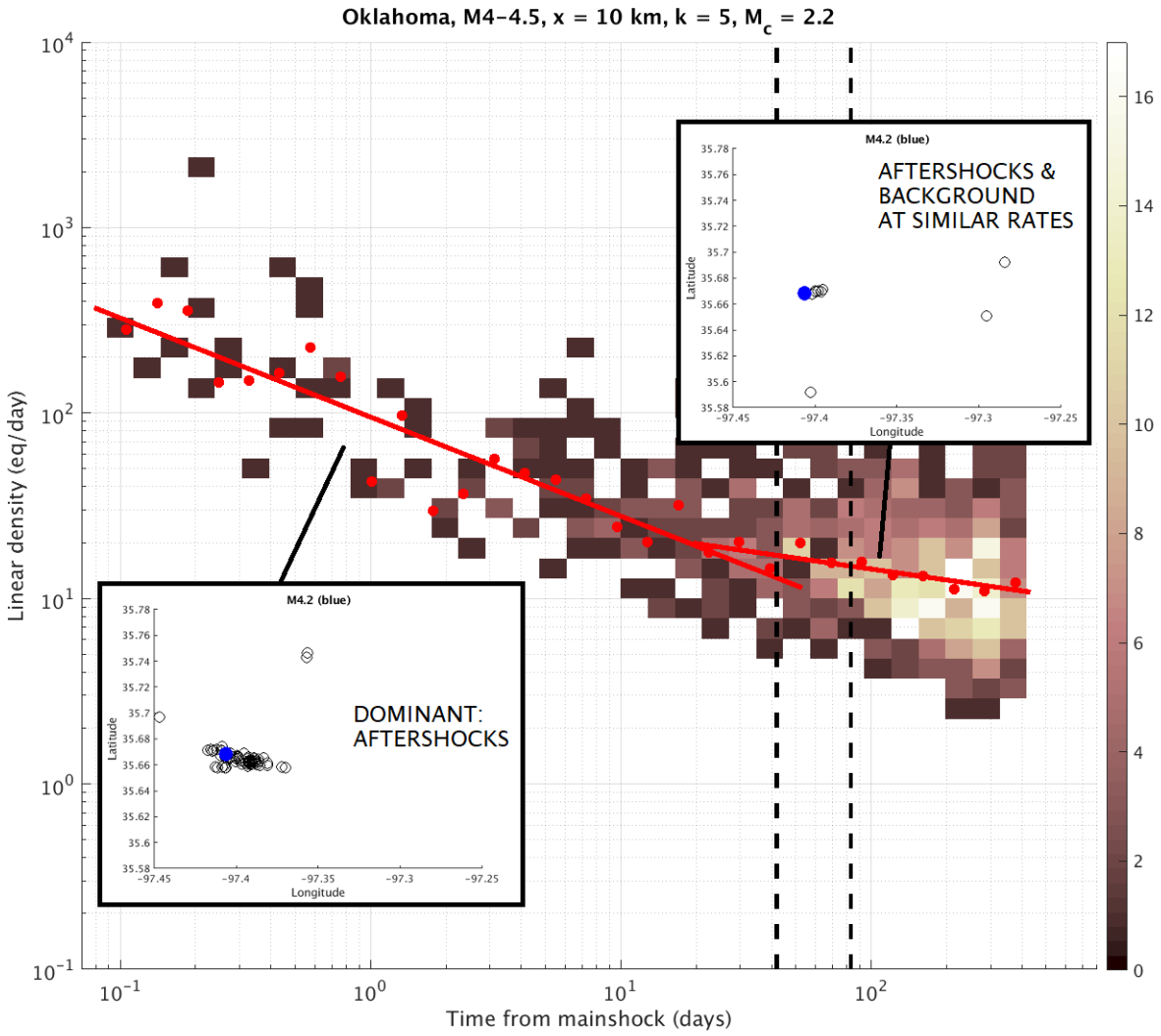

Figure 22. Zoom-in of Figure 21a and conceptual figure to illustrate the two modes of the "expanded spatial window" approach. Left: dominant aftershock rates. Right: aftershocks and background at indistinguishable rates.

4.3 Physical and Geologic Interpretations

Using *p*-values, we find that temporal aftershock decay is indistinguishable between Oklahoma and Southern California (Chapter 4.1). Our temporal decay result is consistent with other statistical studies of Oklahoma seismicity (Llenos & Michael, 2013; Schoenball & Ellsworth, 2017a; Walter et al., 2017), which found that aftershock decay rates for possibly induced mainshocks are not distinguishable from tectonic mainshocks. Inferring underlying physical mechanisms using *p*-values may not be statistically significant given the small sample size in Oklahoma (n=11) and wide range of observed *p*-values in both regions (Figure 13).

Using our data-driven approach to estimate aftershock durations after moderately large mainshocks in Oklahoma, we find agreement with aftershock time windows of *Gardner & Knopoff* (1974), which was derived for Southern California seismicity. This implies that recent Oklahoma aftershock periods are similar to tectonic sequences in Southern California along an active plate boundary. However, this also assumes that the time windows of *Gardner & Knopoff* (1974) accurately describe aftershock duration in Southern California. Additionally, even though shorter aftershock periods in an intraplate region such as Oklahoma may contradict tectonic rate-and-state theory (Dieterich, 1994; Stein & Liu, 2009), induced stresses are likely controlling most of the seismicity rate evolution, so the rate-and-state behavior in Oklahoma cannot be validated or invalidated based on our results.

It has been suggested that slow underlying tectonic loading may increase the effects of stress transfer (Li et al., 2009). If true, this means that pressure perturbations from injection-rate changes related to pore pressure diffusion and poroelasticity have been the strongest control on aftershock productivity (Goebel et al., 2017; McNamara et al., 2015; Walsh & Zoback, 2015). We compile all aftershock sequences without discriminating causal mechanisms or injection-rate

influences, so this observation of potentially rapid aftershock durations in Oklahoma could possibly be considered an averaged representation of some or all these effects.

Chapter 5: Implications for Hazard Modeling

Given that declustering directly determines the rate used for rate-based seismicity forecasting, our study highlights improvements that could be made when declustering Oklahoma earthquake catalogs with window-based methods. We find that the spatial extent of aftershocks in Oklahoma is overestimated by ~20-30 km when using the windows of *Gardner & Knopoff* (1974), which causes seismicity independent of the mainshock to be treated as dependent and discarded from contributing to the Poissonian activity rate. For example, Figure 23 shows that the *Gardner & Knopoff* (1974) window causes the 2016/11/06 M_w 5.0 Cushing, OK mainshock to be considered an aftershock of the Pawnee mainshock and thus removed. Windowing with this method, as done by the USGS (Petersen et al., 2016, 2017, 2018), produces catalogs that are "overly-declustered" and likely reduces the amount of the background activity to be used in the hazard estimation. Thus, the USGS may have consistently underestimated seismic hazard in Oklahoma in their recent one-year forecasts. Our preferred spatial declustering model (Equation 1, Figure 11) more accurately identifies aftershocks in Oklahoma than *Gardner & Knopoff* (1974) as used by the USGS. However, given the results of Chapter 4.2 of this study, the time windows of *Gardner & Knopoff* (1974) are likely sufficient for temporal declustering.

Although a major goal of this study is constraining aftershock windows in Oklahoma, completely accurate aftershock identification is impossible since it relies on a pre-defined conceptual model of a mainshock and its parameters (van Stiphout et al., 2012). Additionally, we

have found that window-based declustering is highly sensitive to background leakage and secondary aftershocks. Fixed windowing methods are best suited for regions with minimal secondary triggering like the mid-continental U.S., including Oklahoma and surrounding states. In general, our study suggests that a detailed review of declustering windows and their limitations is prudent before applying the model to a given region.

To assess if our declustering windows produce a Poissonian background rate, we decluster the Oklahoma catalog using the *Gardner & Knopoff* (1974) and our preferred method (Figures 24 and 25). We find years-long periods where the declustered seismicity rate is several times larger than the historical background rate, exhibiting several years-long rate changes over the last decade. This observation is qualitatively similar to other studies (e.g. Ellsworth, 2013; Walsh & Zoback, 2015). Overall, the background rate appears to be changing relatively rapidly, possibly in response to but not necessarily in synchronicity with changing injection volumes. Although there appears to be 4 distinct periods of relatively constant background rates, a long-term Poissonian assumption is likely invalid.

In general, there is a growing body of evidence questioning whether earthquakes follow a true Poisson process (Corral, 2004; Mulargia et al., 2017) as is assumed in probabilistic seismic hazard assessment (PSHA) (Cornell, 1968; Frankel et al., 1996). Even when catalogs are declustered with common methods and region-specific parameters, they do not consistently fit a Poissonian assumption (Luen & Stark, 2012; van Stiphout et al., 2012). In Oklahoma, where relatively rapid changes in the background rate have occurred, PSHA-type forecasting might be invalid, especially given the short time periods in consideration. Rather, forecast models that incorporate rate-and-state friction responses to variations in wastewater injection changes might yield more accurate forecasting (e.g. Dempsey & Riffault, 2019).

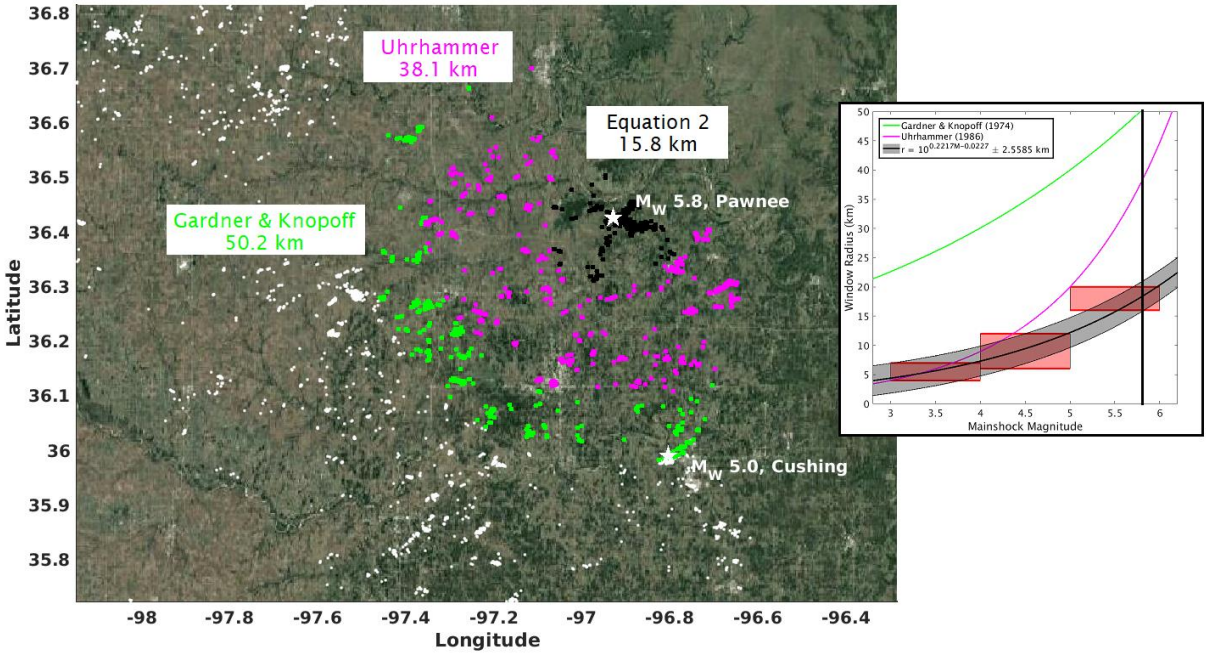

Figure 23. Map-view representation of spatial identification windows around the 2016/09/03 M_w 5.8 Pawnee, OK mainshock. One-year of aftershocks (black, purple, and green) and background (white) are plotted. Inset shows empirical model as in Figure 11, with the solid black line representing the M_w 5.8 mainshock and the window radius values it intersects.

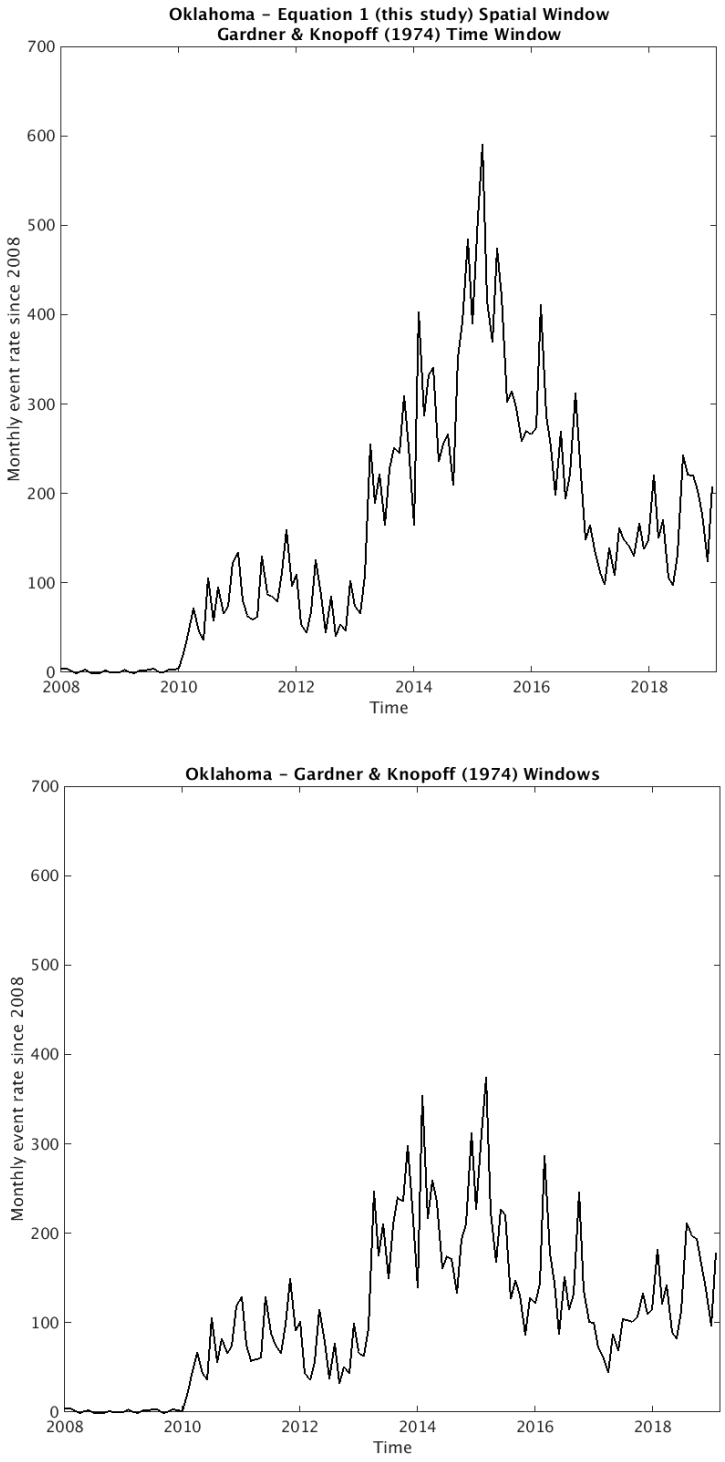

Figure 24. Monthly rates of events above M_c = 2.2 for two declustered Oklahoma catalogs since 2008. All mainshocks above *M* 2.7 have their aftershocks declustered.

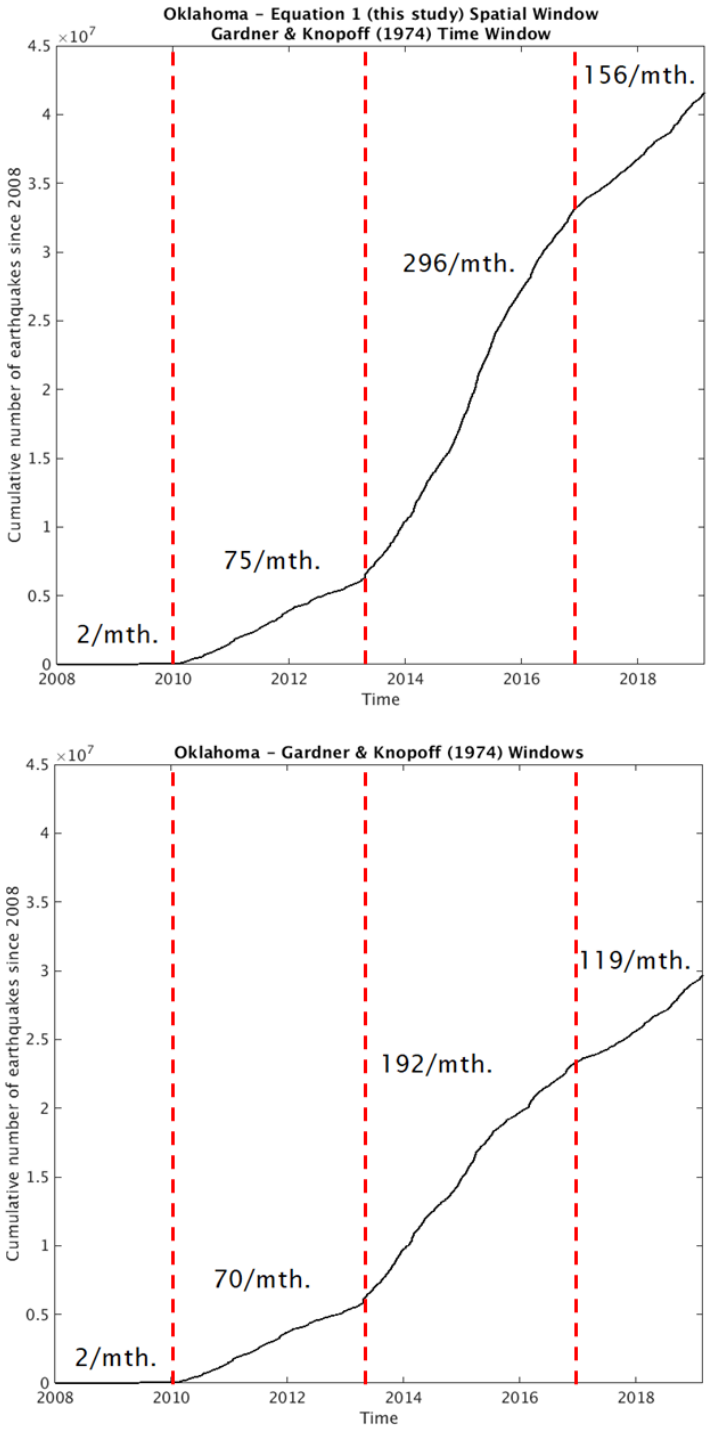

Figure 25. Same declustered catalogs as Figure 24 with the cumulative number of events over time. Red dashed lines separate 4 periods of approximately constant seismicity rates of *M* 2.2 and greater background earthquakes.

Chapter 6: Future Work

An avenue of future research could include comparisons of declustering methods for Oklahoma and in general. A study by *van Stiphout et al.* (2012) showed that both windowing approaches (e.g. Gardner & Knopoff, 1974; Uhrhammer, 1986) had comparable results for establishing a Poissonian background rate as more advanced statistical and stochastic methods (e.g. Zaliapin et al., 2008; Zhuang et al., 2002). However, PSHA has only historically utilized fixed declustering windows. To better understand aftershock physics and clustering behavior in time and space, limitations of both classes of declustering need to be studied in more detail.

Given the issues with both declustering and the Poissonian assumption of earthquakes as described in Chapter 5, some researchers have begun to assess if PSHA should instead utilize non-declustered catalogs (e.g. Petersen et al., 2018). Furthermore, multiple physics-based forecasting models of induced seismicity incorporate catalog data with varying amounts of attention to the use of declustered versus non-declustered catalogs. These recent efforts drive at a larger open question: do aftershocks or background earthquakes drive the seismic hazard of a region?

Chapter 7: Conclusions

We compare spatial and temporal aftershock decay in Oklahoma and Southern California using mainshock-magnitude dependent, space-time windows. We find that spatial aftershock density decays more rapidly in Oklahoma than Southern California. This may be controlled by differences in the physical or geologic conditions of the fault networks in the two regions. Aftershock decay with respect to time is statistically indistinguishable between Oklahoma and California. Understanding how rapidly aftershocks decay in space and time in Oklahoma allows us to constrain the parameters used to define aftershock identification windows.

Our results speak to the need to test the sensitivity of declustering parameters, especially given the impact of background seismicity leakage on aftershock decay rates and thus aftershock windows. We also find that fixed windowing is problematic in regions with productive secondary aftershock triggering and is best applied in intraplate regions with low strain rates and minimal secondary activity. These findings are important for any type of fixed window declustering which has been used in probabilistic seismic hazard assessment.

We find that the *Gardner & Knopoff* (1974) declustering parameters, as used by the USGS in their recent one-year hazard forecasts, overestimate spatial aftershock windows by ~20-30 km and remove thousands of independent earthquakes. Thus, the USGS has been underestimating the background rate and consequently the seismic hazard in Oklahoma given the assumptions in their current framework. Using a declustered catalog with our refined spatial aftershock windows, we find a constant background rate of 156 M 2.2 and greater background earthquakes per month since 2017. Although the background rate has decreased since 2016, Oklahoma seismic hazard will likely remain elevated over the next decade, significantly above the pre-2008 historical background rate of just a few M 3 or greater earthquakes per year.

References

Baker, T. (2017). Looking Ahead: New Earthquake Directive Takes Aim at Future Disposal Rates. https://www.occeweb.com/News/2017/02-24-17%20FUTURE%20DISPOSAL.pdf, (accessed 26 April, 2019)

Baiesi, M., & Paczuski, M. (2004). Scale-free networks of earthquakes and aftershocks. *Physical Review E - Statistical Physics, Plasmas, Fluids, and Related Interdisciplinary Topics*, *69*(6), 8. https://doi.org/10.1103/PhysRevE.69.066106

Benz, H. M., McMahon, N. D., Aster, R. C., McNamara, D. E., & Harris, D. B. (2015). Hundreds of Earthquakes per Day: The 2014 Guthrie, Oklahoma, Earthquake Sequence. *Seismological Research Letters*, *86*(5), 1318–1325. https://doi.org/10.1785/0220150019

Chen, X., Haffener, J., Goebel, T. H. W., Meng, X., Peng, Z., & Chang, J. C. (2018). Temporal correlation between seismic moment and injection volume for an induced earthquake sequence in central Oklahoma. *Journal of Geophysical Research: Solid Earth*, (2016), 1–18. https://doi.org/10.1002/2017JB014694

Chen, X., Nakata, N., Pennington, C., Haffener, J., Chang, J. C., He, X., … Walter, J. I. (2017). The Pawnee earthquake as a result of the interplay among injection, faults and foreshocks. *Scientific Reports*, *7*(1), 1–18. https://doi.org/10.1038/s41598-017-04992-z

Cornell, B. Y. C. A. (1968). Engineering Seismic Risk Analysis. *Bulletin of the Seismological Society of America*, *58*(5), 1583–1606.

Corral, A. (2004). Long-Term Clustering, Scaling, and Universality in the Temporal Occurrence of Earthquakes. *Phys. Rev. Lett., 92(108501)*. https://doi.org/10.1103/PhysRevLett.92.108501

Dempsey, D., & Riffault, J. (2019). Response of Induced Seismicity to Injection Rate Reduction: Models of Delay, Decay, Quiescence, Recovery, and Oklahoma. *Water Resources Research*, *55*(1), 656–681. https://doi.org/10.1029/2018WR023587

Dieterich, J. (1994). A constitutive law for rate of earthquake production and its application to earthquake clustering. *Journal of Geophysical Research*, *99*(B2), 2601–2618.

https://doi.org/10.1029/93JB02581

Ellsworth, W. L. (2013). Injection-Induced Earthquakes. *Science*, *341*. https://doi.org/10.1785/gssrl.83.2.250

Ellsworth, W. L., Llenos, A. L., McGarr, A. F., Michael, A. J., Rubinstein, J. L., Mueller, C. S., … Calais, E. (2015). Increasing seismicity in the U. S. midcontinent: Implications for earthquake hazard. *The Leading Edge*, *34*(6), 618–626. https://doi.org/10.1190/tle34060618.1

Felzer, K R, & Brodsky, E. E. (2006). Decay of aftershock density with distance indicates triggering by dynamic stress. *Nature*, *441*(7094), 735–7388. https://doi.org/10.1038/nature04799

Felzer, Karen R., Abercrombie, R. E., & Ekström, G. (2003). Secondary aftershocks and their importance for aftershock forecasting. *Bulletin of the Seismological Society of America*, *93*(4), 1433–1448. https://doi.org/10.1785/0120020229

Frankel, A., Mueller, C., Barnhard, T., Perkins, D., Leyendecker, E. V., Dickman, N., … Hopper, M. (1996). National Seismic-Hazard Maps: Documentation June 1996. *Open-File Report (USGS), 96-532*.

Galis, M., Ampuero, J. P., Mai, P. M., & Cappa, F. (2017). Induced seismicity provides insight into why earthquake ruptures stop. *Science Advances*, *3*(12). https://doi.org/10.1126/sciadv.aap7528

Gardner, J. K., & Knopoff, L. (1974). Is the sequence of earthquakes in Southern California, with aftershocks removed, Poissonian? *Bulletin of the Seismological Society of America*, *64*(5), 1363–1367. https://doi.org/10.1785/0120160029

Goebel, T. H. W., Walter, J. I., Murray, K. E., & Brodsky, E. E. (2016). Comment on "How will induced seismicity in Oklahoma respond to decreased saltwater injection rates?" by C. Langenbruch and M. D. Zoback. *Science Advances*, *2*(11), e1601542-e1601542. https://doi.org/10.1126/sciadv.1601542

Goebel, T. H.W., Weingarten, M., Chen, X., Haffener, J., & Brodsky, E. E. (2017). The 2016 Mw5.1 Fairview, Oklahoma earthquakes: Evidence for long-range poroelastic triggering at

>40 km from fluid disposal wells. *Earth and Planetary Science Letters*, *472*, 50–61. https://doi.org/10.1016/j.epsl.2017.05.011

Gulia, L., Wiemer, S., & Wyss, M. (2012). Theme IV–Understanding Seismicity Catalog artifacts and quality control. *Community Online Resource for Statistical Seismicity Analysis*, (February), 1–26. https://doi.org/10.5078/corssa-93722864.

Kanamori, H., & Brodsky, E. E. (2004). The physics of earthquakes. *Reports on Progress in Physics*, *67*(8), 1429–1496. https://doi.org/10.1088/0034-4885/67/8/R03

Langenbruch, C., & Zoback, M. D. (2016). How will induced seismicity in Oklahoma respond to decreased saltwater injection rates? *Science Advances*, *2*(11), e1601542–e1601542. https://doi.org/10.1126/sciadv.1601542

Langenbruch, C., Weingarten, M., Zoback, M. D. (2018). Physics-based forecasting of man-made earthquake hazards in Oklahoma and Kansas. *Nature Communications, 9, 3946.* https://doi.org/10.1038/s41467-018-06167-4

Li, Q., Liu, M., & Stein, S. (2009). Spatiotemporal complexity of continental intraplate seismicity. Insights from geodynamic modeling and implications for seismic hazard estimation. *Bull. Seismol. Soc. Am., 99*. 52-60.

Llenos, A. L., & Michael, A. J. (2013). Modeling earthquake rate changes in Oklahoma and Arkansas: Possible Signatures of induced seismicity. *Bulletin of the Seismological Society of America*, *103*(5), 2850–2861. https://doi.org/10.1785/0120130017

Marsan, D., & Lengliné, O. (2010). A new estimation of the decay of aftershock density with distance to the mainshock. *Journal of Geophysical Research: Solid Earth*, *115*(9), 1–16. https://doi.org/10.1029/2009JB007119

McGarr, A. (2014). Maximum magnitude earthquakes induced by fluid injection. *Journal of Geophysical Research: Solid Earth*, 1–12. https://doi.org/10.1002/2013JB010597.Received

McGarr, A., & Barbour, A. J. (2017). Wastewater Disposal and the Earthquake Sequences During 2016 Near Fairview, Pawnee, and Cushing, Oklahoma. *Geophysical Research Letters*, *44*(18), 9330–9336. https://doi.org/10.1002/2017GL075258

McMahon, N. D., Aster, R. C., Yeck, W. L., McNamara, D. E., & Benz, H. M. (2017). Spatiotemporal evolution of the 2011 Prague, Oklahoma, aftershock sequence revealed using subspace detection and relocation. *Geophysical Research Letters*, *44*(14), 7149–7158. https://doi.org/10.1002/2017GL072944

McNamara, D. E., Benz, H. M., Herrmann, R. B., Bergman, E. A., Earle, P., Holland, A., … Gassner, A. (2015). Earthquake hypocenters and focal mechanisms in central Oklahoma reveal a complex system of reactivated subsurface strike-slip faulting. *Geophysical Research Letters*, *42*(8), 2742–2749. https://doi.org/10.1002/2014GL062730

Mulargia, F., Stark, P. B., Geller, R. J. (2017). Why is Probabilistic Seismic Hazard Analysis (PSHA) still used? *Physics of the Earth and Planetary Interiors*, *264*, 63-75. https://doi.org/10.1016/j.pepi.2016.12.002

Newman, A., Stein, S., Weber, J., Engeln, J., Mao, A., & Dixon, T. (1999). Slow deformation and lower seismic hazard at the New Madrid seismic zone. *Science, 284*, 619-621. https://doi.org/10.1126/science/284.5414.619

Norbeck, J. H., & Rubinstein, J. L. (2018). Hydromechanical Earthquake Nucleation Model Forecasts Onset, Peak, and Falling Rates of Induced Seismicity in Oklahoma and Kansas. *Geophysical Research Letters*, *45*(7), 2963–2975. https://doi.org/10.1002/2017GL076562

Ogata, Y. (1999). Seismicity Analysis through Point-process Modeling: A Review. *Pure and Applied Geophysics*, *155*(2–4), 471–507. https://doi.org/10.1007/s000240050275

Pailoplee, S., & Choowong, M. (2014). Earthquake frequency-magnitude distribution and fractal dimension in mainland Southeast Asia. *Earth, Planets and Space*, *66*(1), 1–10. https://doi.org/10.1186/1880-5981-66-8

Pennington, C., & Chen, X. (2017). Coulomb Stress Interactions during the M_w 5.8 Pawnee Sequence. *Seismological Research Letters*, *88*(4), 1024–1031. https://doi.org/10.1785/0220170011

Petersen, M. D., Mueller, C. S., Moschetti, M. P., Hoover, S. M., Llenos, A. L., Ellsworth, W. L., … Rukstales, K. S. (2016). 2016 One-Year Seismic Hazard Forecast for the Central and Eastern United States from Induced and Natural Earthquakes. *Open-File Report*, (June), 1–

50. https://doi.org/10.3133/OFR20161035

Petersen, M. D., Mueller, C. S., Moschetti, M. P., Hoover, S. M., Shumway, A. M., McNamara, D. E., … Rukstales, K. S. (2017). 2017 One-Year Seismic-Hazard Forecast for the Central and Eastern United States from Induced and Natural Earthquakes. *Seismological Research Letters*, *88*(3), 772–783. https://doi.org/10.1785/0220170005

Petersen, M. D., Mueller, C. S., Moschetti, M. P., Hoover, S. M., Shumway, A. M., McNamara, D. E., … Rukstales, K. S. (2018). 2018 One-Year Seismic-Hazard Forecast for the Central and Eastern United States from Induced and Natural Earthquakes. *Seismological Research Letters*. https://doi.org/10.1785/0220170005

Qin, Y., Chen, X., Carpenter, B. M., & Kolawole, F. (2018). Coulomb stress transfer influences fault reactivation in areas of wastewater injection. *Geophysical Research Letters, 45, 11059-11067. https://doi.org/10.1029/2018GL079713*

Reasenberg, P. (1985). Second-order moment of central California seismicity, 1969-1982. *Journal of Geophysical Research: Solid Earth*, *90*(B7), 5479–5495.

Richards-Dinger, K., Stein, R. S., Toda, S. (2010). Decay of aftershock density with distance does not indicate triggering by dynamic stress. *Nature, 467*, 583-586.

Schoenball, M., & Ellsworth, W. L. (2017a). A Systematic Assessment of the Spatio-Temporal Evolution of Fault Activation Through Induced Seismicity in Oklahoma and Southern Kansas. *Journal of Geophysical Research: Solid Earth*, 1–18. https://doi.org/10.1002/2017JB014850

Schoenball, M., & Ellsworth, W. L. (2017b). Waveform-Relocated Earthquake Catalog for Oklahoma and Southern Kansas Illuminates the Regional Fault Network. *Seismological Research Letters*, *88*(5), 7. https://doi.org/10.1785/0220170083

Schorlemmer, D., & Woessner, J. (2008). Probability of detecting an earthquake. *Bulletin of the Seismological Society of America*, *98*(5), 2103–2117. https://doi.org/10.1785/0120070105

Shearer, P., Hauksson, E., & Lin, G. (2005). Southern California hypocenter relocation with waveform cross-correlation, part 2: Results using source-specific station terms and cluster analysis. *Bulletin of the Seismological Society of America*, *95*(3), 904–915.

https://doi.org/10.1785/0120040168

Silverman, B. W. (1986). Density Estimation for Statistics and Data Analysis. *Chapman and Hall, New York.*

Stein, S., & Liu, M. (2009). Long aftershock sequences within continents and implications for earthquake hazard and assessment. *Nature*, *462*, 87-89.

Toda, S., & Stein, R. S. (2018). Why Aftershock Duration Matters for Probabilistic Seismic Hazard Assessment. *Bulletin of the Seismological Society of America*, *108*(3A), 1414–1426. https://doi.org/10.1785/0120170270

Uhrhammer, R. (1986). Characteristics of northern and southern California seismicity. *Earthquake Notes*, *57*, 21.

Utsu, T. (1969). Aftershocks and Earthquake Statistics (I) Some Parameters Which Characterize an Aftershock Sequence and Their Interrelations. *Journal of the Faculty of Science*.

Utsu, T., Ogata, Y., S, R., & Matsu'ura. (1995). The Centenary of the Omori Formula for a Decay Law of Aftershock Activity. *Journal of Physics of the Earth*, *43*(1), 1–33. https://doi.org/10.4294/jpe1952.43.1

van Stiphout, T., Zhuang, J., & Marsan, D. (2012). Seismicity Declustering. *Community Online Resource for Statistical Seismicity Analysis*, (February), 1–25. https://doi.org/10.5078/corssa-52382934.

Walsh, F. R., & Zoback, M. D. (2015). Oklahoma's recent earthquakes and saltwater disposal. *Science Advances*, *1*(5), e1500195–e1500195. https://doi.org/10.1126/sciadv.1500195

Walter, J. I., Chang, J. C., & Dotray, P. J. (2017). Foreshock Seismicity Suggests Gradual Differential Stress Increase in the Months Prior to the 3 September 2016 M w 5.8 Pawnee Earthquake. *Seismological Research Letters*, *88*(4), 1032–1039. https://doi.org/10.1785/0220170007

Wells, D. L., & Coppersmith, K. J. (1994). New Empirical Relationships among Magnitude, Rupture Length, Rupture Width, Rupture Area, and Surface Displacement. *Bulletin of the Seismological Society of America*, *84*(4), 974–1002.

Woessner, J., & Wiemer, S. (2005). Assessing the quality of earthquake catalogues: Estimating the magnitude of completeness and its uncertainty. *Bulletin of the Seismological Society of America*, *95*(2), 684–698. https://doi.org/10.1785/0120040007

Wyss, M., Sammis, C. G., Nadeau, R. M., & Wiemer, S. (2004). Fractal dimension and b-value on creeping and locked patches of the San Andreas fault near Parkfield, California. *Bulletin of the Seismological Society of America*, *94*(2), 410–421. https://doi.org/10.1785/0120030054

Yeck, W. L., Block, L. V., Wood, C. K., King, V. M. (2015). Maximum magnitude estimations of induced earthquakes at Paradox Valley, Colorado, from cumulative injection volume and geometry of seismicity clusters, *Geophys. J. Int., 200,* 322-336. https://doi.org/10.1093/gji/ggu394

Yeck, W. L., Hayes, G. P., McNamara, D. E., Rubinstein, J. L., Barnhart, W. D., Earle, P. S., & Benz, H. M. (2017). Oklahoma experiences largest earthquake during ongoing regional wastewater injection hazard mitigation efforts. *Geophysical Research Letters*, *44*(2), 711–717. https://doi.org/10.1002/2016GL071685

Zaliapin, I., Gabrielov, A., Keilis-Borok, V., & Wong, H. (2008). Clustering analysis of seismicity and aftershock identification. *Physical Review Letters*, *101*(1), 4–7. https://doi.org/10.1103/PhysRevLett.101.018501

Zhuang, J., Ogata, Y., Vere-Jones, D. (2002). Stochastic declustering of space-time earthquake occurrences. *J. Am. Stat. Assoc., 97,* 369-380.

Ziv, A. (2006). Does aftershock duration scale with mainshock size? *Geophysical Research Letters*, *33*(17), 1–5. https://doi.org/10.1029/2006GL027141

Appendix: Spatial Aftershock Decay Tests

The following are the individual spatial aftershock decay plots for *M* 3-5 mainshocks in Oklahoma and Southern California for the parameters used in Figure 8 and Table 2.

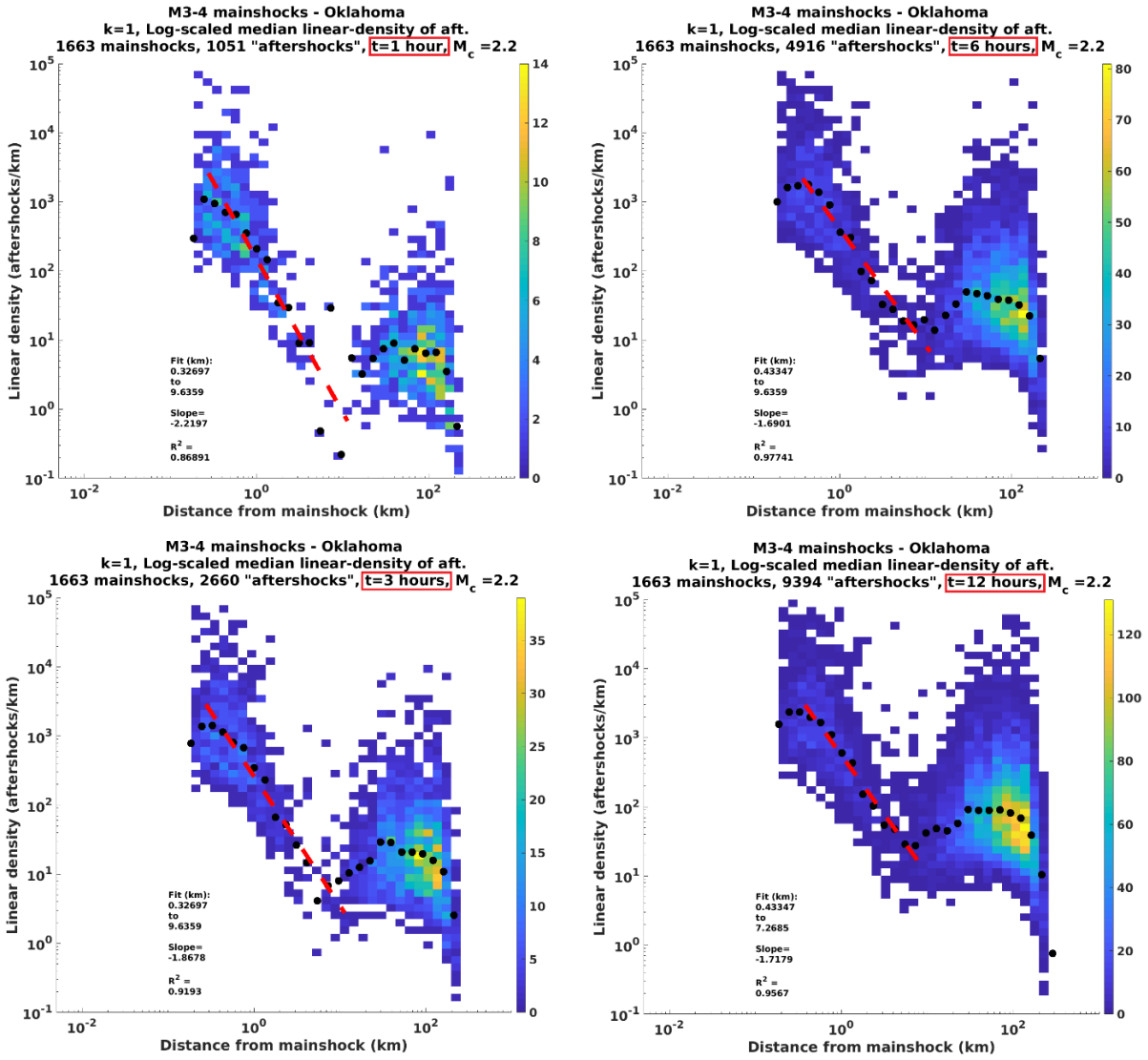

Figure 26. Spatial aftershock decay for mainshocks of $3 \leq M < 4$ in Oklahoma for t = 1 to 12 hours.

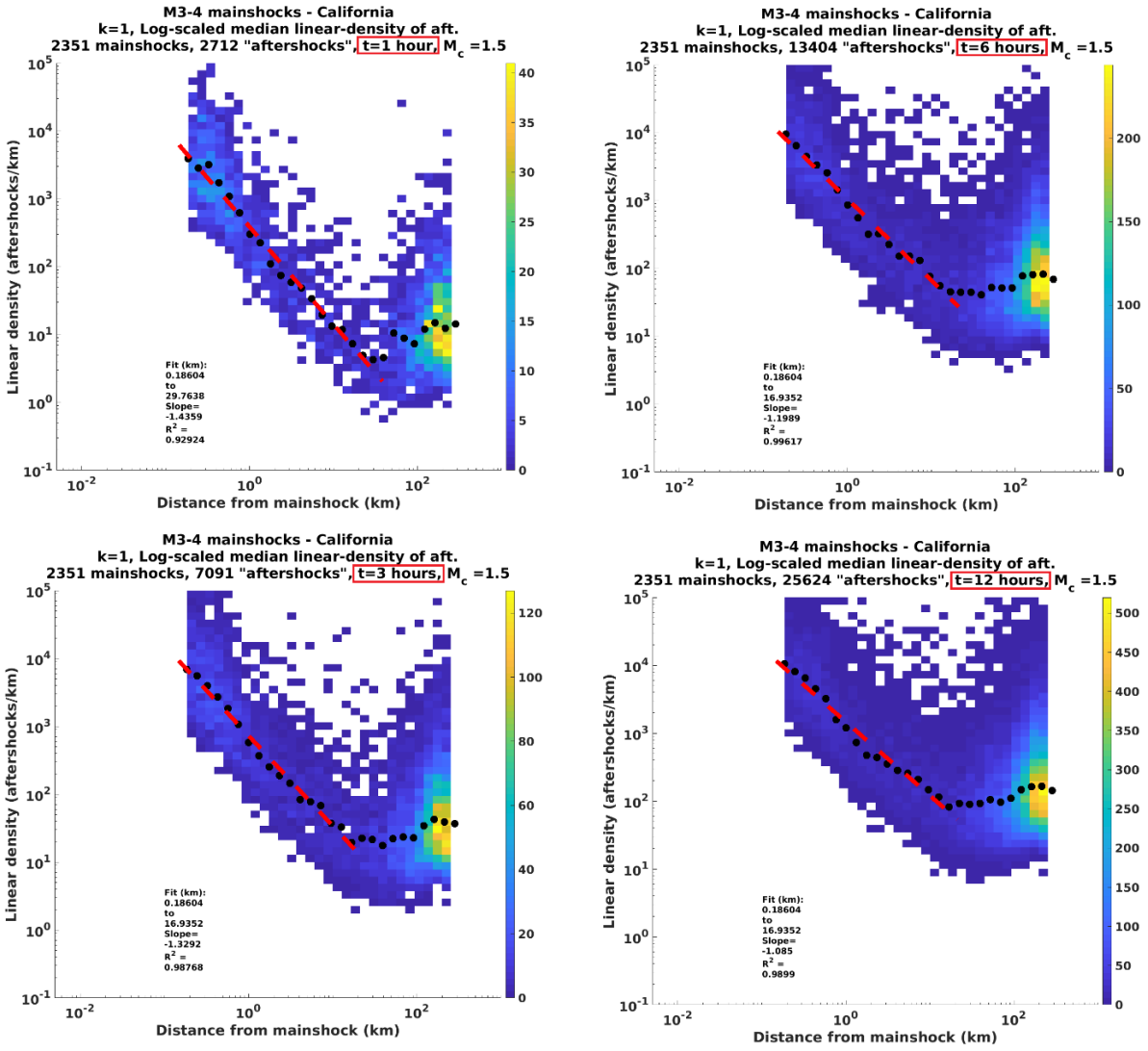

Figure 27. Spatial aftershock decay for mainshocks of $3 \leq M < 4$ in California for t = 1 to 12 hours.

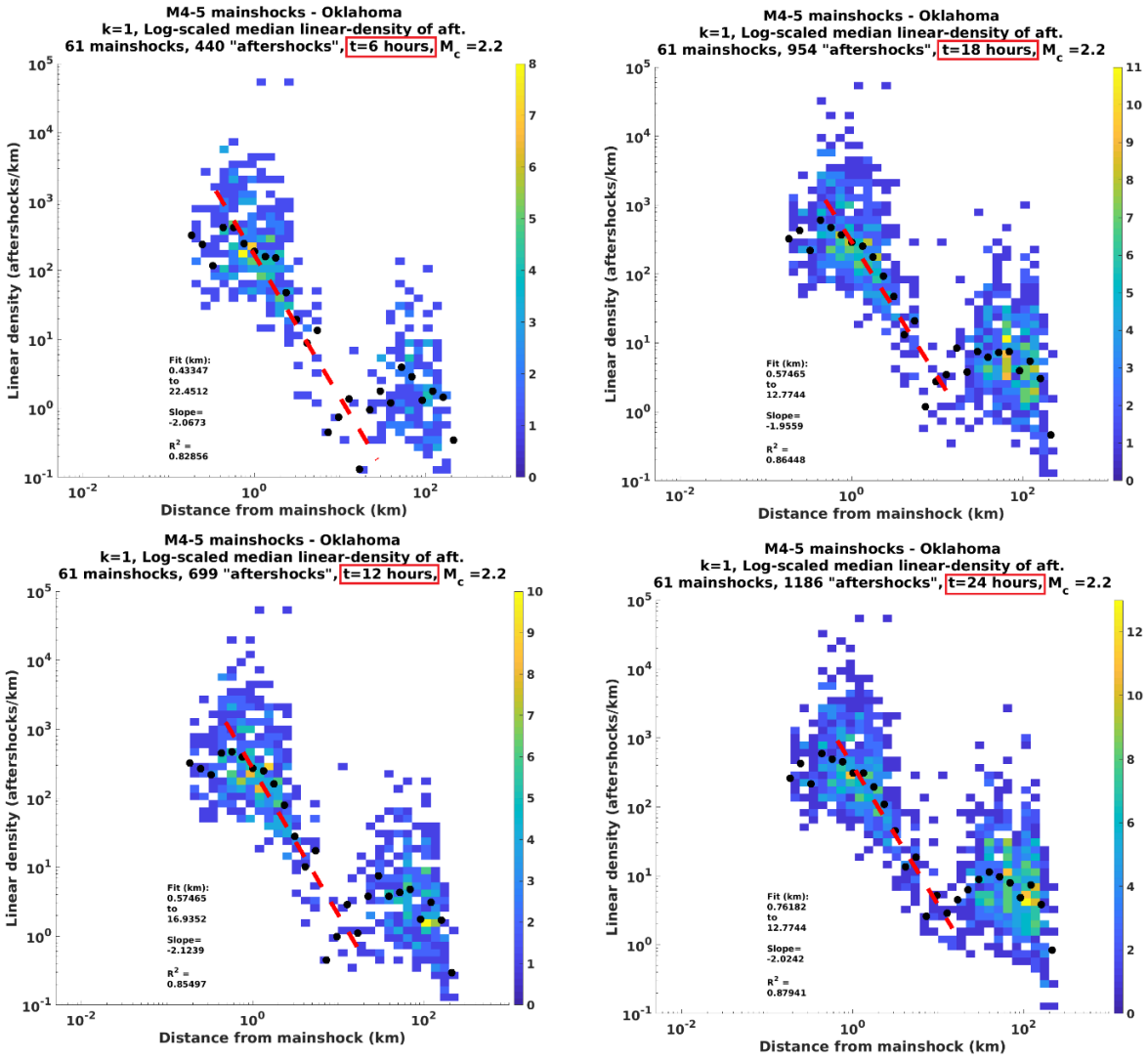

Figure 28. Spatial aftershock decay for mainshocks of $4 \leq M < 5$ in Oklahoma for t = 6 to 24 hours.

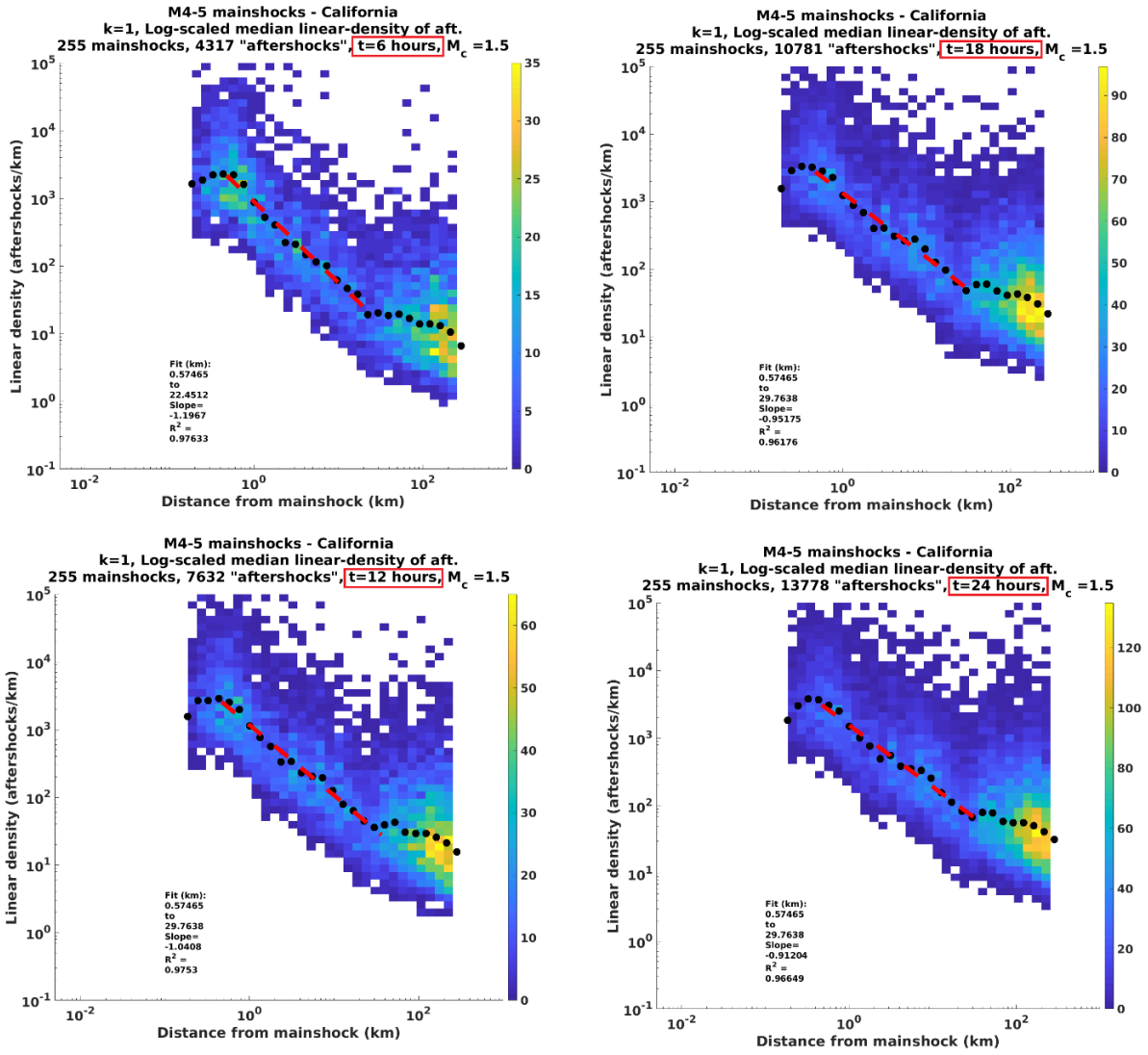

Figure 29. Spatial aftershock decay for mainshocks of $4 \leq M < 5$ in California for t = 6 to 24 hours.